Tracing marine cryptotephras in the North Atlantic during the Last Glacial Period: Protocols for identification, characterisation and evaluating depositional controls

Peter M. Abbott[1,2,3,*], Adam J. Griggs[1], Anna J. Bourne[1,4], Siwan M. Davies[1]

[1]Department of Geography, College of Science, Swansea University, Singleton Park, Swansea, SA2 8PP, UK

[2]School of Earth and Ocean Sciences, Cardiff University, Park Place, CF10 3AT, Cardiff, UK

[3]Institute of Geological Sciences and Oeschger Center for Climate Change Research, University of Bern, Baltzerstrasse 1+3, Bern 3012, Switzerland

[4]Geography and Environment, University of Southampton, University Road, Southampton, SO17 1BJ, UK

*Corresponding author (abbottp@cardiff.ac.uk)

Abstract

Tephrochronology is increasingly being utilised as a key tool for improving chronological models and correlating disparate palaeoclimatic sequences. For many sedimentary environments, however, there is an increased recognition that a range of processes may impart a delay in deposition and/or rework tephra. These processes can affect the integrity of tephra deposits as time-synchronous markers, therefore, it is crucial to assess their isochronous nature, especially when cryptotephras are investigated in a dynamic marine environment. A methodology for the identification and characterisation of marine cryptotephras alongside a protocol for assessing their integrity is outlined. This methodology

was applied to a wide network of North Atlantic marine sequences covering the last glacial period. A diverse range of cryptotephra deposits were identified and, based on similarities in physical characteristics (e.g. glass shard concentration profiles and geochemical homogeneity/heterogeneity), indicative of common modes of tephra delivery and post-depositional reworking, a deposit type classification scheme was defined. The presence and dominance of different deposit types within each core allowed an assessment of spatial and temporal controls on tephra deposition and preservation. Overall, isochronous horizons can be identified across a large portion of the North Atlantic due to preferential atmospheric dispersal patterns. However, the variable influence of ice-rafting processes and an interplay between the high eruptive frequency of Iceland and relatively lower sedimentation rates can also create complex tephrostratigraphies in this sector. Sites within a wide sector to the south and east of Iceland have the greatest potential to be repositories for isochronous horizons that can facilitate the synchronisation of palaeoclimatic records.

Keywords: Quaternary; palaeoceanography; tephrochronology; North Atlantic; transport and deposition; marine cores; glass shard concentrations

1. Introduction

Deposits of volcanic ash, tephra, can act as time-synchronous marker horizons linking palaeoclimatic sequences to help improve chronological models and assess the relative timing of climatic changes (Lowe, 2011). Two fundamental principles that underpin the application of tephrochronology are the rapid deposition of ash at all sites, i.e. instantaneous in geological terms, and that the stratigraphic position of the ash in a sequence directly relates to the timing of the volcanic eruption. Processes that either delay the transportation of ash

51 particles to a site or rework the material following initial deposition can have major impacts
52 on the integrity of deposits as well-resolved isochronous markers. The operation of such
53 processes has been investigated in many sedimentary environments (e.g. Ruddiman and
54 Glover, 1972; Austin et al., 2004; Davies et al., 2007; Brendryen et al., 2010; Payne and
55 Gehrels, 2010; Pouget et al., 2014; Todd et al., 2014; Hopkins et al., 2015; Watson et al.,
56 2015; Zawalna-Geer et al., 2016) and are particularly crucial for cryptotephras, due to the
57 absence of any visible stratigraphic features that would identify the position of the isochron,
58 and hence the timing of deposition, and draw attention to any post-depositional reworking
59 (Davies, 2015). For the marine environment it is critical to consider these processes due to its
60 dynamic nature and the wide range of potential influences, especially when investigating
61 sediments from glacial periods and high-latitude settings where ice-rafting processes could be
62 a significant complicating factor.
63
64 Isochronous tephra deposits are formed in the marine environment if primary tephra fallout is
65 deposited on the ocean surface, rapidly transported through the water column, deposited on
66 the seabed and then preserved in the sediment by subsequent marine sedimentation (Figure
67 1). However, deposition onto other surfaces, e.g. ice sheets and sea-ice, subsequent rafting,
68 and post-depositional reworking and redistribution processes, such as bioturbation and
69 sedimentary loading, can have a major impact on the integrity of tephra deposits in this
70 environment (Figure 1). For instance, these processes can affect the stratigraphic position of a
71 tephra, a pertinent issue for marine sequences due to their lower resolution relative to other
72 records, and potentially compromise the use of the deposit as an isochron. Therefore, it is
73 essential that a full assessment of the sedimentation and depositional processes influencing
74 the preservation, form and isochronous nature of marine cryptotephra deposits is undertaken.

This is especially important if tephra or cryptotephra horizons are to be used as tie lines to assess the relative timing of climatic changes between depositional environments.

Here we present an optimised protocol for marine cryptotephra studies that builds on previous studies, such as, Austin et al. (2004), Brendryen et al. (2010), Abbott et al. (2011, 2013, 2014, 2016), Davies et al. (2014) and Griggs et al. (2014), which used similar methods and indicators to assess visible or cryptotephra deposits within single core sequences. Our examples are derived from a range of depositional settings in the North Atlantic region (Figure 2), but the methodological approach could be applicable to many other marine settings. Within our approach, cryptotephras are identified and characterised using density separation, magnetic separation and electron probe micro-analysis (EPMA) techniques. We then employ a series of indicators to assess the isochronous nature of tephra deposits in the North Atlantic. These include (i) high-resolution shard concentration profiles, (ii) glass shard size variations, (iii) comprehensive single-shard geochemical analysis, and (iv), when available, co-variance with ice-rafted debris (IRD). With a focus on the time-period between 60-25 cal ka BP in the North Atlantic we define several key types of cryptotephra deposit. These are manifested as variations in glass shard concentrations, that share characteristics, such as shard concentrations profiles and geochemical compositions, which are interpreted as being indicative of common transport, depositional and post-depositional processes. The cryptotephra deposit types provide a basis for assessing the dominant controls on tephra deposition in different areas and time periods. Given the widespread core network employed in this study we pinpoint sectors of the North Atlantic Ocean that preferentially preserve isochronous deposits and these underpin a marine tephra framework presented in Abbott et al. (in revision). These horizons are the most valuable for establishing independent high-

precision correlations to the Greenland ice-core records to assess the relative timing of abrupt climate changes.

2. Methodology

2.1 Core Network

Thirteen marine sequences are included in our core network and each record was investigated using the same methodological approach (Figures 2 and 3; Table 1). Cores with well-developed proxy records were prioritised due to the overarching goal of assessing the relative timing of abrupt climate changes during the last glacial period. In addition, cores from areas with high sedimentation rates and sufficient material for contiguous tephra sampling were selected. Overall the network has a wide geographical spread. However, in some instances paired cores from nearby locations were investigated to assess the stratigraphic integrity of individual tephra deposits. It was not always possible to fulfil all of these requirements. For instance, contiguous samples were not available from MD95-2024 and two sites, M23485-1 and GIK23415-9, do not have well-resolved records of abrupt climate changes. However, these sites were included to increase the geographical extent and capture a wide range of depositional settings.

2.2 Identification of cryptotephra deposits

Cryptotephras were identified and characterised according to the methodological protocol outlined in Figure 3. Although most aspects of this marine-focussed methodological approach have been described separately in previous studies, here we synthesise the full procedure.

Core sequences were initially analysed at a low-resolution (5 or 10 cm sampling intervals) using contiguous samples, i.e. samples taken along the whole length of depth intervals with no gaps between samples, to provide an initial quantified assessment of tephra content (i.e. glass shards) for the whole period of interest. Selected intervals were then reanalysed at a high-resolution (1 cm depth intervals) depending on a range of factors, outlined in Section 3, consistent with other studies of both marine and terrestrial sequences (e.g. Pilcher and Hall, 1992; Lane et al., 2015; Matthews et al., 2015). Both low and high-resolution samples were processed according to the workflow outlined in Figure 3.

Within the protocol, samples are sieved to isolate glass shards in three recommended size fractions (>125 µm, 80-125 µm and 25-80 µm). This separation and focus on fine-grain sizes is a development from prior studies that focused on coarser grain size fractions (e.g. >150 µm - Austin et al., 2004, Voelker and Haflidason, 2015; 63-125 µm and 125-150 µm – Brendryen et al., 2010), most typically utilised in the identification of foraminifera. The development was driven by the increased identification of cryptotephras as fine-grained deposits in distal sequences (Davies, 2015). The smallest grain-size fraction (25-80 µm) was split using heavy liquid separation into density fractions most likely to contain glass shards, a method initially developed to identify tephras or cryptotephras in terrestrial sediments (Hodder and Wilson, 1976; Turney, 1998; Blockley et al., 2005). Magnetic separation is an additional step utilised to separate paramagnetic basaltic material from minerogenic material with a similar high density (>2.5g/cm^3; Griggs et al., 2014). Whilst magnetic separation is infrequently employed for terrestrial sequences, e.g. Mackie et al. (2002), it is routinely applied in this investigation to aid the isolation and identification of basaltic glass. The high number and proportion of basaltic horizons, relative to rhyolitic horizons, identified in this study demonstrates the value of including this step of magnetic separation within marine cryptotephra studies in the North

149 Atlantic. During low-resolution analysis, magnetic separation was only utilised on the 25-80
150 µm size fraction, because the time required for this process was longer than the time required
151 to count shards from an unseparated sample of the coarser-grained fractions. However, during
152 preparation of samples for geochemical analysis these coarse-grained fractions were
153 magnetically separated alongside the 25-80 µm fraction to provide a purer basaltic glass
154 sample.
155
156 If a low-resolution tephrostratigraphy was being constructed, all fractions were inspected for
157 glass shard content using optical microscopy (i.e. >125 µm, 80-125 µm, 2.3-2.5 g/cm^3 and
158 the >2.5 g/cm^3 magnetic fraction; step 12 in Figure 3). However, when glass shard
159 concentration profiles were refined at a higher 1 cm sampling resolution, some fractions were
160 not inspected. For example, if no rhyolitic material was present at a low resolution then the
161 2.3-2.5 g/cm^3 fraction was not inspected.
162
163 Depending on the nature of the samples and the glass contained within a sequence, alternative
164 or additional steps were occasionally adopted (Figure 3). For instance, in some cores
165 sediment clusters, that appear to consist of sediment bound together by biogenic silica, were
166 observed (see also Ponomareva et al., 2018). These clusters were broken down using a weak
167 treatment of sodium hydroxide (NaOH) (step 5). This chemical treatment could also be
168 undertaken after step 3 of the method if clusters are known to be present following initial
169 investigations. In such cases, the HCl should be washed out of the sediments, but no re-
170 sieving is necessary. NaOH has previously been used in cryptotephra studies to remove
171 biogenic silicates (e.g. Rose et al., 1996), with samples warmed to 90°C for 4 hours.
172 However, it was found that treatment at room temperature for 1 hr was sufficient to
173 disaggregate the sediment clusters in this study. As a precaution, NaOH treatment was

avoided when samples were being prepared for geochemical analysis, as it has been suggested that NaOH could cause geochemical modification (e.g. Blockley et al., 2005). However, other studies have shown that such treatments do not affect the glass composition (e.g. Steinhauser and Bichler, 2008) and experimentation by Ponomareva et al. (2018) indicates that electron-probe micro analysis (EPMA) analyses are unaffected by this weak NaOH treatment.

To quantify exceptionally high shard concentrations (~>10,000 per 0.5 g dry weight sediment (dws)), samples were spiked with Lycopodium spore tablets containing a known quantity of pollen grains (step 10 in Figure 3). The threshold of 10,000 glass shards per 0.5 g dws is recommended as this roughly equivalent to the number of pollen spores present in a tablet. The ratio between glass shards and pollen grains is then used to quantify shard concentrations (e.g. Griggs et al., 2014). This is an adaption of a standard pollen counting approach previously applied to tephra and cryptotephra studies by Gehrels et al. (2006). Typically, it is not known if this quantification approach is required until low-resolution analysis has been conducted. Hence, if high shard concentrations were observed in low-resolution samples and it became apparent that shard concentrations would exceed 10,000 shards, then counting was halted and the additional step of spiking samples was incorporated into high resolution analysis of those sections.

2.3 Geochemical analysis of cryptotephra deposits

Shard concentration profiles are employed to select samples for geochemical analysis using the criteria outlined in Section 3. Samples were re-processed using steps 1-9 of the procedure in Figure 3, but, the fractions of interest were then mounted in epoxy resin on 28 × 48 mm

199 microprobe slides to permit the sectioning of the glass shards (Figure 3). When high shard
200 concentrations were present, all material from the fraction was mounted directly on to the
201 slides. When glass shards were present only at a low concentration (~<50 per 0.5 g dws) they
202 were picked onto a microprobe slide using a micromanipulator. Shards prepared by this
203 method are easier to locate during sectioning and EPMA analysis. Flat and polished sections
204 through the individual glass shards were produced for EPMA analysis using decreasing
205 grades of silicon carbide paper and 9, 6 and 1 µm diamond suspensions.
206
207 EPMA was conducted at the Tephra Analytical Unit, University of Edinburgh, using a
208 Cameca SX100 with five wavelength dispersive spectrometers over a number of analytical
209 periods. All shards were analysed using the same operating conditions outlined in Hayward
210 (2012). Pure metals, synthetic oxides and silicate standards were used for calibration. The
211 secondary standards of Cannetto Lami Lava, Lipari and BCR2g were analysed at regular
212 intervals to monitor for instrumental drift within analytical sessions, to assess the precision
213 and accuracy of analysed samples and to provide a cross-check of the comparability of
214 analyses between analytical periods. A comparatively large number of shards (~20-40
215 individual shards) were analysed for each deposit to provide comprehensive characterisations
216 that underpin the assessment of taphonomic processes, depositional controls and the
217 isochronous nature of deposits. For all analysis and data comparison the major element data
218 were normalised to an anhydrous basis, i.e. 100 % total oxides. However, the geochemical
219 data utilised here are provided as raw analyses in the Supplementary Data alongside
220 secondary standard analyses.
221
222 ***3. Constructing a tephrostratigraphy***
223

The two major indicators that we employ to assess the integrity of marine tephra deposits are (i) contiguous high-resolution shard concentration profiles and (ii) rigorous geochemical characterisation of the glass shards. These are the key aspects of the tephrostratigraphies defined in this work. Constructing a tephrostratigraphy, however, involves a series of selections and we illustrate our approach, which aimed for consistency and comparability between cores, with reference to the record of brown (basaltic) shards in the MD99-2251 core from the Iceland Basin between 1650-1950 cm depth (Figure 4). There was a distinct lack of colourless shards in this core section but a slight increase was observed towards the base, which can be related to reworking and redistribution of the underlying North Atlantic Ash Zone II (NAAZ) II (see Section 4).

First a low-resolution shard concentration profile is constructed to determine the overall presence of cryptotephra and to define the background level of glass shards within a sequence (e.g. Figure 4a). All notable shard peaks were then re-analysed at a high-resolution (1 cm sampling interval) to refine their stratigraphic position. This step is crucial because the peak in concentration is typically thought to represent the timing of atmospheric fallout from a volcanic event (e.g. Ruddiman and Glover, 1972; Jennings et al., 2002; Davies et al., 2012). Theoretically it is possible for the maximum shard concentration peak to lie below the original depth of deposition, based on an interplay of the extent of mixing within and depth of the mixing layer and the sedimentation rate at the site, but, the impact of such mixing has been assessed as negligible in practice (Berger and Heath, 1968; Ruddiman and Glover, 1972). Indeed, our focus on high sedimentation rate sites would negate this effect, however, it is recommended that the potential influence of mixing on the isochron position is considered for individual horizons if they are to be used as isochronous tie-lines between sequences.

249 Selecting which peaks to refine at a 1 cm sampling resolution depends on the peak versus
250 background concentrations, the shape and discreteness of peaks and replication across grain-
251 size fractions (e.g. Figure 4a). To some extent there is subjectivity in the selection of peaks
252 and no consistent concentration thresholds could be defined because of variability in peak
253 and background shard concentrations both within and between the core sequences. In most
254 instances, but not exclusively, shard concentrations in the 25-80 μm fraction displayed the
255 greatest variability and occurrence within the records and were the prime criteria for these
256 selections (e.g. Figure 4a). For some cores, high-resolution investigations were extended over
257 intervals wider than the main peaks to provide a greater constraint on shard concentration
258 variations (e.g. between 1678-1698 cm in MD99-2251; Figure 4a) and/or additional samples
259 were analysed to determine if smaller peaks were due to increased input of material from a
260 volcanic event or general fluctuations in background shard concentrations (e.g. between
261 1869-1874 cm and 1879-1884 cm in MD99-2251; Figure 4a). In addition, the time required
262 for processing and analysing the number of selected samples was considered.
263
264 Reanalysing selected sections at a high-resolution allows an integrated shard concentration
265 profile to be constructed (e.g. Figure 4b) that, in general, constrains the shard peaks to
266 vertical distances of 1 or 2 cm in a core, and higher concentrations were normally observed in
267 the high-resolution counts (e.g. peaks at 1680-1681 cm and 1904-1905 cm depth in MD99-
268 2251; Figure 4b). This observation was anticipated because the low-resolution counts should
269 provide an average of the glass shard concentration over the sampling interval and has been
270 observed for other cores within the network. However, in some cases lower peak
271 concentrations or very few shards were observed in the high-resolution samples (e.g. the
272 1869-1874 and 1879-1884 cm sections in MD99-2251; Figure 4b). This mis-match may be
273 due to uneven lateral distribution of glass shards within core sequences, a lack of horizontal

continuity or glass shards being constrained in pods or lenses. Glass shard distributions of this nature have been observed in thin section (2D) and X-ray microtomography (3D) analysis of North Atlantic marine tephra sediments (Griggs et al., 2014, 2015). These additional 2D and 3D methods can provide further sedimentological information to aid isochron placement and the interpretation of post-depositional processes, however, at present they have not been widely applied to tephra deposits in our network.

Once an integrated tephrostratigraphy is defined, shard peaks are selected for geochemical analysis to allow the assessment of volcanic source and deposit integrity. Peaks were selected using criteria akin to those used to pinpoint samples for high-resolution analysis, i.e., discreteness relative to background concentrations, replication across grain-size fractions and processing and analysis time (e.g. Figure 4b). On occasions, glass shards from long upward tails in deposition or secondary peaks were analysed to provide further insights into the nature of individual deposits (see Section 4.1).

4. Results

4.1 Classification of individual tephra deposits

We utilised the approach outlined above to construct a tephrostratigraphic record for all cores within our network and tephra deposits were identified in the vast majority of records. Glass shard concentration profiles, geochemical characterisations and other indicators, such as shard size and co-variance with IRD, were integrated for these cryptotephra deposits to define a deposit type classification scheme (Table 2). Six deposit types that each share similar physical characteristics reflecting common modes of delivery and post-depositional

299 reworking are identified (Table 2). This classification scheme is mainly based on deposits of
300 brown glass shards (i.e. basaltic material) due to the relative lack of colourless shard deposits.
301 However, Type 3, is an exception and is based on deposits that are most commonly
302 associated with colourless shards related to NAAZ II, the most widespread silicic tephra
303 found within our core network.
304
305 Deposit Types 1,2 and 3 are all characterised by distinct concentration peaks, however, their
306 profiles vary in form, displaying discrete (e.g. Figure 5a(i)), bell-shaped (e.g. Figure 6a(i))
307 and asymmetric (e.g. Figure 7a(i)) forms, respectively, and in vertical spread ranging from 1
308 cm to up to 100 cm (Table 2). These contrasting features are attributed to variable shard
309 concentrations between the deposit types and differential influence of post-depositional
310 reworking. For instance, the low shard concentrations of Type 1 deposits contribute towards
311 their discreteness. Whilst this discreteness may result from limited post-depositional
312 reworking, it is also possible that the low concentration of glass shards deposited at the sea-
313 bed is not an adequate tracer of such activity. Reworking such as bioturbation, however,
314 would most likely not impact the isochron position (see Section 3). In contrast, the higher
315 glass shard concentrations associated with Type 2 deposits allows the glass shards to act as a
316 tracer for bioturbation (e.g. Ruddiman and Glover, 1972; Griggs et al., 2015), which creates
317 the upward and downward tails in deposition and roughly bell-shaped profile. This shard
318 distribution pattern has often been viewed as the classic form of tephra deposits preserved in
319 marine records (e.g. Ruddiman and Glover, 1972).
320
321 For Type 3 deposits the extremely high shard concentrations rapidly isolated underlying
322 sediment from bioturbative activity and restricted downward migration of shards, as observed
323 for the FMAZ II deposit in Griggs et al. (2015). The upward tail and continued deposition of

glass is primarily attributed to secondary deposition of glass shards from the same volcanic event from the surrounding sea-bed due to bottom current transportation. Bioturbative reworking may have also contributed towards increasing the overall vertical spread of these deposits. In combination these two factors create the observed asymmetric profile (e.g. Figure 7a(i); Table 2). Additional samples in the overall declining concentration profile of Type 3 deposits were sometimes analysed, particularly when subsidiary peaks were observed, in case any subsequent volcanic events were obscured within the upward tail. In all instances these additional analyses had an identical composition to shards in the main peak, corroborating the assertion that the upward tail was formed mainly through reworking of material from a single eruption (e.g. Figure 7a(i)).

Deposit Types 1, 2 and 3 are most likely derived from single depositional events, yet their isochronous nature can only be fully determined by assessing the relative homo/heterogeneity of their geochemical signature. Type 1 and 3 deposits have a homogeneous major element signature, i.e. all analysed shards form a single geochemical population most likely sourced from one volcanic eruption, which strongly suggests that they were deposited via primary fall and are useful isochronous tephra markers (e.g. Figure 5a(ii) for Type 1 deposits and Figure 7a(i) for a Type 3 deposit). Type 2 deposits are sub-divided into Type 2A, which have a homogeneous composition, and Type 2B, which have a heterogeneous composition with the analysed shards forming multiple populations and/or revealing a wide spread of analyses with high variability and limited consistency. Figures 6a and 6b provide examples of homogeneity based on major element analyses for two Type 2A deposits, whilst, Figure 5b provides examples of the heterogeneity observed for two Type 2B deposits. This sub-categorisation is important as the homogeneous Type 2A deposits are likely to be isochronous, akin to Type 1 and 3 deposits, while the heterogeneity of Type 2B deposits most likely reflects the

deposition of products from multiple eruptions and probably secondary transport processes that affect the isochronous nature of the horizons. For example, geochemical heterogeneity is a key indicator of transport via iceberg rafting and/or the amalgamation of the products of closely timed eruptions (Griggs et al., 2014). An additional line of evidence for Type 2B deposits is co-variance of shard concentrations with IRD records. The relative proportion of shards across the different grain-size fractions can also help determine transport processes because sea-ice rafting typically transports shards larger than would be expected via primary fallout to distal sites (e.g. Austin et al., 2004). Overall, for Type 2 deposits a careful assessment of a range of key indicators is required to determine their value as isochronous deposits.

In contrast to the single concentration peaks displayed by deposit Types 1, 2 and 3, Type 4 deposits display multiple peaks over a period of elevated shard concentrations whereas Type 5 deposits are characterised by glass shards in multiple consecutive samples, but with no clear pattern or peaks in shard concentrations (Table 2). In most cases, the multiple peaks seen in the Type 4 deposits display similar major element geochemical signatures but they are typically heterogeneous, e.g. the 456-473 cm depth deposit widely dispersed in MD04-2820CQ (Figure 7b; Abbott et al., 2016). This compositional pattern indicates that the entire deposit is an amalgamation of eruptive material from several, closely-timed, volcanic eruptions and that the multiple peaks are the product of secondary transport processes (e.g. bioturbation and bottom current reworking) rather than primary fallout. Alternatively, the glass shards found in Type 4 deposits may have been amalgamated during deposition on the Icelandic ice-sheet and subsequently transported to core sites via iceberg rafting. As with Type 2B deposits, further insights into the mode of deposition may be gained by comparing shard concentration profiles with iceberg rafting proxies. Without a distinct concentration

374 peak or geochemical evidence that they were sourced from a single eruption, Type 4 deposits
375 typically cannot be utilised as isochronous marker horizons for high-precision correlations.
376 However, they have the potential to be used as regional marine-marine core tie-lines, as
377 suggested for FMAZ III by Abbott et al. (2016).
378
379 Type 5 deposits are commonly identified during low-resolution investigations. Only selected
380 deposits were re-evaluated at a high-resolution and for geochemical composition. No distinct
381 concentration peaks were identified, and geochemical analyses revealed heterogeneous
382 populations of shards that were geochemically identical to those of underlying deposits, e.g.
383 NAAZ II. As such, Type 5 deposits are interpreted as a background of glass shards that are
384 deposited at the core sites and dispersed in the sediment column by remobilisation and
385 reworking processes. These background signals vary between sites and may mask and
386 hamper the identification of primary fall events that resulted in deposition of glass shards
387 only in low concentrations. High-resolution analysis coupled with intensive geochemical
388 characterisation may isolate such events and would be appropriate if specific volcanic events
389 were being targeted. However, this was not feasible within our extensive core network.
390
391 *4.2 Categorising core sequences using the tephra classification scheme*
392
393 The tephra classification scheme has been employed to categorise the cores according to the
394 presence and dominance of different deposit types. Four core categories have been identified
395 (Figure 8) and range from sites dominated by primary fall deposits (sites marked in green) to
396 sites with deposits affected by secondary processes (sites marked in red). In addition, very
397 few shards were identified in the northernmost (JM04-25PC from the Western Svalbard
398 slope) and southernmost (MD01-2444 from the Iberian Margin) records. Trace amounts (1-2

399 shards) were identified in some low-resolution samples but none were replicated as
400 significant deposits during high-resolution analysis.
401
402 *4.2.1 Core dominated by Type 1 deposits*
403
404 Only two marine sequences exclusively contain Type 1 deposits, MD04-2822 from the
405 Rockall Trough and MD04-2829CQ from the Rosemary Bank (Figure 8). The Type 1
406 deposits comprise discrete peaks in brown shard concentrations constrained vertically within
407 ~1 cm and both sites have a limited background of brown shards over the zone of interest
408 (e.g. Figure 5a(i)). Shards from the discrete peaks have single homogeneous geochemical
409 populations that can be directly related to single volcanic source regions (Figure 5a(ii)) and
410 hence likely represent isochronous marker horizons. The shard concentrations were low (~5-
411 40 shards per 0.5 g dws in the 25-80 μm fraction) and occasionally replicating these peaks to
412 extract shards for geochemical analysis was challenging. This lack of replication may be a
413 consequence of the uneven distribution of shards within the cores. However, the successful
414 identification of these Type 1 deposits does demonstrate how the approach adopted in this
415 work can be used to trace such low concentration deposits.
416
417 *4.2.2 Cores containing single occurrences of Type 2A deposits*
418
419 Two cores, MD95-2010, from the Norwegian Sea, and MD01-2461, from the Porcupine
420 Seabight, each contain just one significant tephra deposit with bell-shaped shard
421 concentration profiles (Figure 6a(i) and b(i)). These deposits were identified because
422 significant numbers of shards were isolated over 10-20 cm intervals in the low-resolution
423 counts. Given their homogeneous geochemical compositions, these are both classified as

Type 2A deposits (Figure 6a(ii) and b(ii)) and are thus thought to be isochronous markers. Evidence of upward reworking within MD01-2461 is seen as a small subsidiary shard peak, positioned 4-5 cm above the highest shard concentrations, with an identical geochemical composition at both depths (Figure 6b). In both cores only trace amounts (<2-3) of shards were present in the rest of the low-resolution samples, apart from ~10 shards identified around NAAZ II in MD95-2010.

4.2.3 Cores containing mixed deposit types

Five of the core sites have been grouped into this category (Figure 8) and contain a range of deposit types. Type 2 deposits dominate and these are typically relatively discrete with high shard concentrations, but the geochemical compositions range between homogeneous (Type 2A) and heterogeneous (Type 2B). Type 4 deposits are also present in some sequences and at most sites the rhyolitic component of NAAZ II is present as a Type 3 deposit. The MD04-2820CQ record is a prime example of this mixed category. It contains a number of Type 2 deposits, with differing geochemical homogeneity, the FMAZ III as a Type 4 deposit and the NAAZ II rhyolitic component as a Type 3 deposit (Abbott et al., 2016). The variability in tephra deposit types means that a careful assessment of individual deposits is required and strongly suggests that the depositional controls at sites in this category varied temporally throughout the last glacial period.

4.2.4 Core dominated by Type 2B and Type 4 deposits

Two cores have been grouped within this category, SU90-24 from the Irminger Basin and M23485-1 from the Iceland Sea (Figure 8). These sites are characterised by multiple glass

concentration peaks within a high background level of shards, e.g. 1,000-10,000s of shards per 0.5 g dws. Peaks in shard concentration are not well-resolved in these records and the distinct contrast between SU90-24 and a Type 1 dominated core (MD04-2822) is shown in Figure 5. For SU90-24, single-shard analyses from some of the concentration peaks have highly heterogeneous geochemical signatures, with a wide range of major oxide values that span several different Icelandic volcanic systems (Figure 5b). Given the shard concentration profiles and compositional results, these deposits are classified as Type 2B and Type 4. M23485-1 is dominated by Type 4 deposits with two major depositional pulses of heterogeneous basaltic and rhyolitic material. Overall, the deposits found in these cores cannot be considered as isochronous horizons.

5. Discussion - Controls on Ash Deposition and Preservation

The core categorisation highlights that a diverse range of tephrostratigraphies were preserved during the last glacial period across the North Atlantic. Geographical clustering of similar core sites suggests that there were both spatial and temporal controls on ash deposition. Various factors could have controlled the transport and deposition of tephra, including (i) the nature of volcanism inputting tephra into the system, (ii) atmospheric dispersal patterns and distance from eruptive source, (iii) rafting by icebergs and sea-ice and (iv) the rate and nature of sedimentation. Local factors may have also operated at individual cores sites. Through an assessment of these factors we propose that for our core categories common controls operating within different sectors of the North Atlantic can be identified (Figure 9).

5.1 Frequency and composition of Icelandic volcanism

474 The marine tephra records are ultimately controlled by the nature and frequency of Icelandic
475 eruptions as these provide the primary input of tephra into the North Atlantic. Currently the
476 most well-resolved record of Icelandic eruptions during the glacial period is derived from the
477 Greenland ice-cores (Bourne et al., 2015) as proximal records are relatively limited due to the
478 removal of material by glacial activity and the burial of deposits by subsequent volcanic
479 activity. Within the Greenland ice-cores over 99 tephra or cryptotephra deposits have been
480 identified in this time-period, which is significantly higher than the number identified within
481 our marine tephra framework but could suggest that some of the marine deposits have
482 amalgamated material from multiple eruptions (e.g. FMAZ III in JM11-19PC and MD04-
483 2820CQ; see Figure 7b). Within our core network there is a greater abundance of basaltic
484 horizons in comparison to rhyolitic deposits, which is consistent with the Greenland ice-core
485 records, where 95 % of the deposits are basaltic (Bourne et al., 2015). This dominance of far-
486 travelled basaltic material within distal sites could be due to the increased ice cover during
487 the last glacial period which implies that the horizons were derived from subglacial
488 phreatomagmatic eruptions, which can enhance the explosivity of basaltic eruptions due to
489 the presence of water (Larsen and Eiríksson, 2008). The relative lack of rhyolitic horizons in
490 the ice-cores suggests that the rhyolitic background of shards observed in many of the marine
491 records is most likely due to reworking of material from NAAZ II, rather than resulting from
492 subsequent volcanic activity.
493
494 *5.2 Atmospheric dispersal patterns and proximity to Iceland*
495
496 Following a volcanic eruption, the wind-driven dispersal patterns will largely dictate the
497 location of fall deposits. The proximity of a core site to the volcano is important as the grain-
498 size, shard concentration and thickness of airfall deposits decreases exponentially away from

499 the eruptive source. Atmospheric transport skews this relationship with extended transport of
500 material along transport axes downwind from the eruptive source and this bias is more
501 evident at distal sites (Sparks et al., 1981; Pyle, 1989; Lacasse, 2001).
502
503 The four cores solely preserving deposits thought to be transported via primary ashfall (i.e.
504 sites marked green and orange containing Type 1 and Type 2A deposits: MD95-2010, MD04-
505 2829CQ, MD04-2822 and MD01-2461; Figure 9) are located between the south and east of
506 Iceland. This oceanic sector stretches from the south coast of Ireland to the west coast of
507 Norway, with the two green sites containing multiple deposits lying close together towards
508 the SE off the west coast of Scotland (Figure 9). Other sites that preserve a mix of deposit
509 types including some deposited via atmospheric transport, i.e. yellow coded sites, also
510 generally lie to the south and east of Iceland with the exception of MD95-2024 (Figure 9).
511 This clustering of sites suggests that tephra was transported from Iceland via westerly winds,
512 consistent with dominant wind patterns and typical plume heights of Icelandic eruptions.
513
514 Modern observations indicate that over Iceland wind direction changes progressively with
515 altitude in the troposphere, with easterlies dominating at ground level shifting to southerly at
516 a low level (1.4 km) and westerlies in the upper troposphere and lower stratosphere between
517 9-15 km throughout the year (Lacasse, 2001). Above 15 km altitude seasonal variability is
518 observed with strong westerlies during the autumn and winter and relatively weak easterlies
519 during the spring and summer (Lacasse, 2001). The modern atmospheric patterns are utilised
520 as an analogue for dispersal of tephra during the glacial period as the reconstruction of glacial
521 wind patterns is uncertain. Studies do suggest, however, that surface circulation was more
522 intense over the North Atlantic during the last glacial period (e.g. Kutzbach and Wright,
523 1985; Mayewski et al., 1994;). Plume heights from modern basaltic eruptions similar in

524 nature to those that occurred during the last glacial period (e.g. Vatnajökull 1996, Hekla
525 2000, Grímsvötn 2004 and 2011 and Eyjafjallajökull 2010) were typically between ~8-15 km
526 with some reaching 25 km altitude (Gudmundsson et al., 2004; Höskuldsson et al., 2007;
527 Kaminski et al., 2011; Oddsson et al., 2012; Petersen et al., 2012). For older eruptions,
528 Lacasse (2001) deduced from proximal and distal grain sizes that the Saksunarvatn Ash,
529 erupted from Grímsvötn in the early Holocene, produced an eruption column of at least 15
530 km elevation. Eruptive plume heights together with dominant wind directions suggest that
531 basaltic tephra was mainly atmospherically transported away from Iceland in an easterly
532 direction, which is consistent with our findings.
533
534 Southward atmospheric dispersal of some tephras, to core sites such as MD99-2251 and
535 MD04-2820CQ, may be a consequence of modification by more variable surface wind
536 conditions that reflect the weather at the time of an eruption (Lacasse, 2001). A similar
537 scenario was observed for the Eyjafjallajökull 2010 eruption, with weather conditions
538 exerting a strong influence following initial easterly transport of tephra (Davies et al., 2010).
539 Other variable influences such as precipitation, the timing of the eruption, style of volcanism,
540 magma discharge rate and height of eruptive column may have also created differences from
541 the general pattern for individual eruptions. Although our observations indicate some
542 dispersal towards the south, no tephra deposits were preserved in the southernmost site
543 MD01-2444, most likely as a consequence of the long distance between this site and the main
544 Icelandic source.
545
546 Preferential atmospheric transport of ash to the east and south of Iceland is also consistent
547 with the identification of tephra fall deposits or cryptotephra deposits from Iceland in
548 terrestrial deposits from sites in northwest Europe (e.g. Lawson et al., 2012) and their absence

549 to the west and southwest of Iceland (e.g. Greenland – Blockley et al., 2015; eastern North
550 America - Pyne-O'Donnell et al., 2012; Mackay et al., 2016). Cryptotephra is preserved at
551 the most westerly site, MD95-2024. This core is downwind and the second farthest from
552 Iceland with greater peak and background shard concentrations relative to closer and
553 downwind sites such as MD04-2829CQ and MD04-2822. This cryptotephra occurrence
554 conflicts with the expected atmospheric dispersal pattern of tephra and proximity to source,
555 strongly indicating that other processes were at times helping to control tephra delivery to the
556 North Atlantic west of Iceland.
557
558 The observation of limited atmospheric dispersal in a northerly direction from Iceland has
559 some conflicts with the observations of Bourne et al. (2015), who inferred direct transport of
560 ash in a north-westerly direction to the Greenland ice-sheet (Figure 9). However, this conflict
561 could be a consequence of marine sites north of Iceland being more dominantly influenced by
562 other controls, such as ice-rafting deposition of tephra (see discussion below), which masked
563 any isochronous primary fall deposits. The distance from source was highly likely to be a
564 dominant control on the non-preservation of tephra at the most northerly site JM04-25PC.
565
566 Overall, therefore, while atmospheric transport was the primary mechanism delivering tephra
567 to the sites marked in green and orange on Figure 9 it was only a partial control on the
568 delivery of tephra to the sites marked in yellow. At those locations other controls had an
569 additional influence, leading to the identification of some diachronous deposits.
570
571 *5.3 Ice-Rafting of Tephra and Ocean Currents*
572

573 The potential for tephra to have been rafted either by sea-ice or icebergs prior to deposition in
574 the glacial North Atlantic has been highlighted previously and this process can transport
575 material along different trajectories and further from the source than atmospheric dispersal.
576 Three distinct areas that preserve tephra deposited by rafting processes, i.e. deposit Types 2B
577 and 4, have been identified. These areas are the Iceland Sea and Irminger Basin to the north
578 and west of Iceland (core sites M23485-1 and SU90-24), the mid Atlantic (MD95-2024,
579 MD99-2251, GIK23415-9, MD04-2820CQ) and northeast of the Faroe Islands (JM11-19PC).
580 Whilst the Iceland Sea and Irminger Basin were heavily influenced by these processes
581 throughout the 60-25 cal ka BP period, both Type 2A and Type 2B deposits were preserved
582 in the other two areas suggesting that the influence of rafting was temporally variable (Figure
583 8).
584
585 Surface ocean currents have a huge role to play in the trajectory of tephra-bearing sea-ice and
586 icebergs away from Iceland (Bigg et al., 1996) and thus influence the deposition of tephra at
587 core sites during melting. Modern surface ocean currents are illustrated on Figure 9 and are
588 used as an approximate analogue for the glacial period. The North Atlantic Drift (NAD) from
589 the southwest dominates the warm surface ocean currents and splits into the Irminger Current
590 south of Greenland and the North Iceland Irminger Current around Iceland before flowing
591 into the Nordic Seas. Cold currents are dominated by the East Greenland Current flowing
592 down the east coast of Greenland. A distinct feature of the surface circulation is the subpolar
593 gyre, an anti-clockwise ocean surface circulation south of Iceland (Figure 9). These surface
594 ocean currents would have strongly influenced ice-rafting but the source of icebergs and sea-
595 ice extent was also an important factor.
596

The expanded size of the LGM ice-sheet over Iceland suggests that ice calving margins could have been located all around the island (Figure 9). With the majority of the major volcanic centres located in the south of the island, icebergs from the southward margin may have contained a greater concentration of tephra, however, local atmospheric transport north, east and west of the volcanoes would have contributed material to icebergs calving from all of these margins. The circulation patterns shown in Figure 9 suggests that icebergs from all margins could have been transported in surface ocean currents. Sea-ice reconstructions have shown that its extent over the North Atlantic region varied in time with the DO and Heinrich events (Hoff et al., 2016). It has been suggested that sea-ice retreated abruptly during the warming at the start of interstadials, but spread rapidly from the coast of Greenland during interstadial cooling with perennial sea-ice extending beyond Iceland during cold stadials and reaching a greater extent during Heinrich events (Figure 9; Hoff et al., 2016). This temporal variability in sea-ice coverage and its rafting along similar trajectories to those proposed for icebergs is likely to have played a role in the dispersal of tephra.

Iceberg rafting from the north coast of Iceland was the likely primary control on tephra deposition north and west of Iceland. The M23485-1 site lies close to the northern margin of the LGM Icelandic ice sheet and icebergs calved from this margin could have been entrained within the East Greenland Current and deposited material over the SU90-24 site. In addition, sea-ice rafting may have contributed towards this pattern of tephra deposition as the latter site lies within the stadial perennial ice-sheet limits and would have been covered early in the advances during interstadial cooling phases. Within the mid-Atlantic area, Icelandic icebergs transported in the subpolar gyre are likely to have deposited material at both the MD95-2024 and MD99-2251 sites. The MD04-2820CQ and GIK23415-9 sites lie within the IRD Belt, an area of the North Atlantic within which IRD from the Laurentide Ice Sheet was deposited

during Heinrich events, and may have been influenced by Icelandic icebergs transported in this zone by surface currents (Figure 9). Indeed, glass shards have been found in association with the lithic Heinrich layers (e.g. Obrochta et al., 2014). The influence of sea-ice rafting in the mid-Atlantic would have been temporally variable throughout the glacial period and hence should not be ruled out as a potential process for ash transport and deposition as MD95-2024 and MD99-2251 lie close to the stadial perennial sea ice limit and MD04-2820CQ and GIK23415-9 lie close to the Heinrich event limit (Figure 9). The area to the northeast of the Faroe Islands, the JM11-19PC site, may have been influenced by both rafting processes, with icebergs transported from the north coast of Iceland in the North Iceland Irminger Current and it lies close to the limit of perennial sea-ice during stadial periods. For all sites potentially affected by rafting processes key indicators such as the level of geochemical heterogeneity and shard sizes should be utilised to assess the origin of individual deposits.

The lack of rafted deposits in the MD04-2822 and MD04-2829CQ cores may be due to the Rockall Trough, the main pathway by which the warm North Atlantic surface water flows northward into the Norwegian Sea, effectively isolating them from the influence of Icelandic icebergs. The sites lie close to the stadial perennial sea ice limit so could be susceptible to sea ice rafting. However, the tephrostratigraphic records strongly indicate that this process has not deposited glass at these particular sites. Continuous sea-ice cover can be ruled out as a potential control on the lack of tephra preservation at the northerly JM04-25PC site. The reconstructed sea-ice limits from Hoff et al. (2016) suggest that although the site is the most northerly, sea-ice cover was limited to stadial phases and Heinrich events and was not greater than at other sites, e.g. SU90-24 and M23485-1, which contain significant cryptotephra deposits (glass shard concentrations) (Figure 9).

647

648 *5.4 Nature and Rate of Sedimentation*

649

650 Sedimentation rates are a further important control on tephra preservation. They provide
651 information on the nature of sedimentation and slower rates of sedimentation increase the
652 likelihood that the products of separate but closely timed eruptions are amalgamated. Table 1
653 presents approximate average sedimentation rates for all the sites in the core network
654 between 60-25 cal ka BP. In general, all the sites had relatively high sedimentation rates, a
655 bias created by our prioritisation of sites to include in the network (see Section 2.1).

656

657 These high sedimentation rates may indicate that, in addition to sedimentation occurring
658 through pelagic settling, bottom currents were also transporting material to the sites (Rebesco
659 et al., 2014). Thus, the sites incorporated in the network may have an increased susceptibility
660 to secondary deposition of tephra-derived glass shards via bottom current reworking. This
661 process could account for the persistent low background levels of glass shards at most sites
662 (Type 5 deposits) and occasional outlying single shard analyses in the cryptotephra deposits
663 (see Abbott et al., in revision). However, bottom current reworking does not appear to have
664 been a significant control on the nature of these tephra records. The only deposit type that we
665 interpret as being formed and affected by bottom current reworking is Type 3, which can be
666 attributed to the exceptionally high peak shard concentrations in comparison to the other
667 deposit types (Table 2). Almost exclusively, Type 3 deposits are NAAZ II occurrences,
668 unique deposits formed by an event that led to the input of a sufficient concentration of
669 shards into the oceanic system to be reworked and act as a tracer for bottom current activity.
670 As with bioturbation, the lack of evidence of reworking for other deposits does not
671 definitively demonstrate that this process was not occurring, because glass shard tephra

concentrations could have been too low to be detected using our methods (i.e. insufficient to act as an adequate tracer).

There is no clear difference in sedimentation rates between the cores containing only isochronous deposits (i.e. green and orange marked sites) and those dominated by heterogeneous secondary deposits (i.e. red marked sites) with estimated rates of 14-20 cm/ka and 17-19 cm/ka respectively (Table 1; Figure 8). However, in general the sites containing a mix of deposit types (yellow marked sites; Figure 8) have lower sedimentation rates, between 9-11 cm/ka, apart from the MD95-2024 site which had a rate of 22 cm/ka (Table 1). This contrast in sedimentation rates is a general reflection of these cores deriving from the deepest sites in the network, away from terrestrial sediment sources and the higher sedimentation rates observed on continental shelves (Figure 9). The low sedimentation rates may have contributed towards the preferential occurrence of Type 2B and Type 4 deposits at these sites due to the increased likelihood of closely spaced eruptive products being amalgamated. With Icelandic basaltic tephra horizons in the Greenland ice-cores having an average recurrence interval of ~1 per 200 years during this period (Bourne et al., 2015), and 200 years being represented by ~2 cm depth at the sites depicted in yellow (Figure 9) it is highly likely that closely spaced eruptions were mixed. The lower sedimentation rates would also have contributed to slower upward migration of the bioturbation mixing zone, promoting the amalgamation of deposits and vertical elongation of the shard concentration profile for Type 2 deposits. Each deposit must be evaluated individually as these sites may also be heavily influenced by rafting processes, which can produce Type 2B deposits with geochemical heterogeneity. Overall, the lower sedimentation rates and thus temporal resolution at all these sites could account for the lower number of cryptotephra horizons identified within the

696 marine core network in comparison to the numbers in the Greenland ice-core records (see
697 Abbott et al., in revision for further discussion).
698
699 *5.5 Local Site Conditions*
700
701 Based on their proximity to Iceland, atmospheric dispersal patterns and tephra rafting in the
702 North Atlantic, it might be expected that MD95-2010 and MD01-2461 would both contain a
703 number of cryptotephra deposits. Each, however, only contained a single tephra deposit, the
704 FMAZ IV in MD95-2010 and NAAZ II in MD01-2461, strongly suggesting that another
705 factor was limiting the deposition of tephra at these sites. Both sites lie close to the former
706 limits of LGM ice sheets and are amongst the shallowest sites in the network (Figure 9; Table
707 1). Higher levels of terrigenous sediment deposition might have masked or diluted the glass
708 shard concentrations at these sites, especially if the non-tephric material was coarse-grained
709 and/or dense because the shard concentrations presented in this work are referenced to
710 sediment mass.
711
712 *5.6 Summary*
713
714 In general, whilst only a small area of the North Atlantic was disposed to solely preserving
715 isochronous Type 1 and Type 2A deposits, these primary tephra-fall deposits can also be
716 preserved in a wide area to the east and south of Iceland due to prevalent atmospheric
717 dispersal patterns. Only a small area to the north and west of Iceland does not preserve any
718 isochronous primary fall deposits. We suggest that the most significant factor complicating
719 the tephrostratigraphic records is the rafting of tephra within icebergs and sea-ice, which can
720 be constrained spatially but also displays temporal variability, particularly at sites within the

central North Atlantic. In addition, the high frequency of Icelandic volcanic eruptions during the period provides a constraint on the number of tephra. Despite our focus on sites with relatively high sedimentation rates, the rates are potentially still too low to enable individual events to be resolved within the sediment cores.

6. Conclusions

This work provides an integrated methodology for the identification of cryptotephras in North Atlantic marine records alongside a protocol for assessing the integrity of deposits and the influence of primary and secondary transport and depositional processes based on a classification scheme for glass shard deposits. A widespread network of cores was studied and six key glass shard deposit types with common physical characteristics and depositional and transport histories were identified in these records. The deposits types range from valuable ash-fall deposited isochronous horizons, to geochemically heterogeneous deposits with complex histories, to persistent background signals of ash deposition. While the variety of deposit types observed in the glacial North Atlantic reflects the complexity of processes controlling the transport, deposition and post-depositional reworking of tephra and may be unique to this setting, the methodological approach for identification could underpin investigations in other oceanic regions.

A regional analysis of the tephrostratigraphic records has shown that a range of different controls influenced tephra deposition and the deposit types preserved as glass-shard concentrations at different sites within the North Atlantic over the last glacial period. A key area to the southeast of Iceland was sheltered from any ice-rafting influence and only isochronous primary fall deposits have been isolated in these records. However, primary

746 deposits were also identified in a wide oceanic sector between the south and east of Iceland,
747 which could be the focus of future studies to identify further isochronous horizons or to
748 extend the distribution of those identified within this work. The wider significance of the
749 isochronous horizons identified in this work is discussed in Abbott et al. (in revision), which
750 defines a framework of marine tephra horizons for the 60-25 cal ka BP period in the North
751 Atlantic region.
752
753 ***Acknowledgements***
754
755 This work was financially supported by the European Research Council (TRACE project)
756 under the European Union's Seventh Framework Programme (FP7/2007-2013) / ERC grant
757 agreement no. [259253]. PMA also acknowledges support from the European Research
758 Council under the European Union's Horizon 2020 research and innovation programme
759 (grant agreement No 656381). We also acknowledge funding by NERC (NE/F020600/1,
760 NE/F02116X/1, NE/F021445/1) for the SMART project which contributed towards the
761 research ideas presented in this work. Thanks are due to William Austin, Henning Bauch,
762 Mark Chapman, Frederique Eynaud, Ian Hall, Claude Hillaire-Marcel, Elisabeth Michel, Tine
763 Rasmussen, Bjørg Risebrobakken, James Scourse, Mara Weinelt and the British Ocean
764 Sediment Core Research Facility (BOSCORF) for providing samples or access to the marine
765 cores utilised within this study. We would like to thank Dr Chris Hayward for his assistance
766 with the use of the electron microprobe at the Tephrochronology Analytical Unit, University
767 of Edinburgh. Thanks also to Gareth James, Gwydion Jones and Kathryn Lacey (Swansea
768 University) for assistance with laboratory processing. We thank David Lowe and an
769 anonymous reviewer for their helpful comments that have improved this manuscript. This
770 paper contributes to the EXTRAS project (EXTending TephRAS as a global geoscientific

771 research tool stratigraphically, spatially, analytically, and temporally within the Quaternary),
772 an INTAV-led project (International Focus Group on Tephrochronology and Volcanism)
773 within the Stratigraphy and Chronology Commission (SACCOM) of the International Union
774 for Quaternary research (INQUA).

775 ***Figures Captions***

776

777 **Figure 1:** Flow chart of the transportation and depositional processes that could have affected
778 tephra within the glacial North Atlantic prior to preservation in marine sediments. Adapted
779 from Griggs et al. (2014).

780

781 **Figure 2:** Network of North Atlantic marine cores studied within this work and ice-cores
782 mentioned within the text.

783

784 **Figure 3:** Flow chart of the consistent methodology utilised to determine the glass shard
785 content of cores within the marine network and to extract and prepare such shards for major
786 element geochemical analysis. NaOH = sodium hydroxide. SPT = sodium polytungstate.

787

788 **Figure 4:** Example of the construction of a tephrostratigraphy using the MD99-2251 core. (a)
789 Low-resolution brown glass shard concentration profiles split into three grain-size fractions.
790 Blue bars denote depth intervals reinvestigated at a 1 cm sampling resolution in the core. (b)
791 Integrated high and low resolution brown shard counts for the MD99-2251 core. Shard counts
792 have been truncated for clarity. Shard counts in the 1686-1687 cm sample (*) are 4991, 1862
793 and 507 shards per 0.5 g dws in the 25-80, 80-125 and >125 µm grain-size fractions,
794 respectively. The shard counts for the 25-80 µm grain-size fraction from the 1904-1905 cm
795 sample (**) are 3776 shards per 0.5 g dws. Red bars denote samples depths from which glass
796 shards were subsequently extracted for compositional characterisation by EPMA.

797

798 **Figure 5:** Comparison of (i) tephrostratigraphic records and (ii) compositional
799 characterisations of glass shard deposits from the (a) MD04-2822 and (b) SU90-24 marine

sequences. Brown shard counts for the 25-80 µm grain-size fraction from 470-500 cm in SU90-24 have been truncated for clarity. Shard counts exceed 40,000 shards per 0.5 g dws, but, two peaks could be identified at 480-481 cm and 486-487 cm. Percentage abundance of *Neogloboquadrina pachyderma* (sinistral) record for MD04-2822 from Hibbert et al. (2010). Magnetic susceptibility record for SU90-24 from Elliot et al. (2001). Geochemical fields for Icelandic source volcanoes are based on normalised whole rock and glass shard analyses utilised in Bourne et al. (2015) and references within and additional data for the Kverkfjöll volcano from Gudmundsdóttir et al. (2016). Within MD04-2822 additional discrete peaks can be observed, e.g. at 1731-1732 cm and 1965-1966 cm. However, it was not possible to acquire sufficient material for geochemical characterisation. All geochemical data plotted on a normalised anhydrous basis.

Figure 6: Examples of shard concentration profiles and geochemical characterisations for Type 2A tephra deposits from two North Atlantic marine records within the network. (a) MD95-2010 (i) 910-920 cm high-resolution tephrostratigraphy of brown glass shards, (ii) compositional variation diagrams of analyses from glass shards extracted from the 915-916 cm depth sample. Chemical classification and nomenclature for total alkalis versus silica plot after Le Maitre et al. (1989) and division line to separate alkaline and sub-alkaline material from MacDonald and Katsura (1964). Geochemical fields for Icelandic tholeiitic volcanic systems defined using normalised whole rock and glass shard analyses from Jakobsson et al. (2008) (Reykjanes), Höskuldsson et al. (2006) and Óladóttir et al. (2011) (Kverkfjöll) and Jakobsson (1979), Haflidason et al. (2000) and Óladóttir et al. (2011) (Grímsvötn and Veidivötn-Bardabunga). (b) MD01-2461 (i) 940-950 cm high-resolution tephrostratigraphy of colourless glass shards (ii) total alkalis versus silica plot of analyses from glass shards extracted from the 947-948 cm depth sample. Normalised compositional fields for the

825 Icelandic rock suites derived from whole rock analyses in Jakobsson et al. (2008). All
826 geochemical data plotted on a normalised anhydrous basis.
827
828 **Figure 7:** Examples of shard concentration profiles and geochemical characterisations for a
829 (a) Type 3 and a (b) Type 4 deposits from two North Atlantic marine records within the
830 network. (a) MD99-2251 (i) 1950-2030 cm tephrostratigraphy of colourless glass shards
831 integrating low and high-resolution shard counts (ii) compositional variation diagrams
832 comparing characterisations of colourless glass shards from 1974-1979 cm and 2014-2015
833 cm depth. (b) MD04-2820CQ (i) 450-480 cm high-resolution tephrostratigraphy of brown
834 glass shards (ii) compositional variation diagrams comparing characterisations from four
835 shard peaks within the Type 4 deposit. Data from Abbott et al. (2016). Chemical
836 classification and nomenclature for total alkalis versus silica plot after Le Maitre et al. (1989)
837 and division line to separate alkaline and sub-alkaline material from MacDonald and Katsura
838 (1964). All geochemical data plotted on a normalised anhydrous basis.
839
840 **Figure 8:** Classification of core sites within the marine core network. See Section 4.2 for
841 details of classes.
842
843 **Figure 9:** Primary controls and influences on the deposition of tephra within the glacial
844 North Atlantic Ocean. Ocean surface currents and names from Voelker and Haflidason
845 (2015) and Rasmussen et al. (2016). Currents: IC = Irminger Current; NIIC = North Iceland
846 Irminger Current; EGC = East Greenland Current; EIC = East Iceland Current; NAD = North
847 Atlantic Drift; SPG = Subpolar Gyre. Last Glacial Maximum (LGM) ice limits from Dyke et
848 al. (2002), Funder et al. (2011) and Hughes et al. (2016). Perennial sea ice limits from Hoff et
849 al. (2016). Core classification from Figure 7.

850

851 **Supplementary Information**

852

853 **Table S1:** Original major oxide concentrations of shards from tephra deposits in the MD04-
854 2822 core. Deposits analysed are from the depths of (i) 1836-1837 cm (ii) 2004-2005 cm and
855 (iii) 2017-2018 cm.

856

857 **Table S2:** Original major oxide concentrations of shards from tephra deposits in the SU90-24
858 core. Deposits analysed are from the depths of (i) 340-342 cm (ii) 420-422 cm (iii) 480-481
859 cm and (iv) 486-487 cm.

860

861 **Table S3:** Original major oxide concentrations of shards from the MD95-2010 915-916 cm
862 tephra deposit.

863

864 **Table S4:** Original major oxide concentrations of shards from MD01-2461 related to the
865 rhyolitic component of North Atlantic Ash Zone II (II-RHY-1). Deposits analyses are at (i)
866 942-943 cm and (ii) 2014-2015 cm depth.

867

868 **Table S5:** Original major oxide concentrations of shards from MD99-2251 related to the
869 rhyolitic component of North Atlantic Ash Zone II (II-RHY-1). Deposits analyses are at (i)
870 1974-1975 cm and (ii) 947-948 cm depth.

871

872 **Table S6a:** Original secondary standard analyses of the BCR2g standard made throughout
873 analytical periods during which sample glass shard analyses presented in this work were
874 analysed.

875

876 **Table S6b:** Original secondary standard analyses of the Lipari standard made throughout

877 analytical periods during which sample glass shard analyses presented in this work were

878 analysed.

879

880 ***References***
881
882 Abbott, P.M., Austin, W.E.N., Davies, S.M., Pearce, N.J.G., Hibbert, F.D., 2013.
883 Cryptotephrochronology of a North East Atlantic marine sequence over Termination II, the
884 Eemian and the last interglacial-glacial transition. Journal of Quaternary Science 28, 501-514.
885
886 Abbott, P.M., Austin, W.E.N., Davies, S.M., Pearce, N.J.G., Rasmussen, T.L., Wastegård, S.,
887 Brendryen, J., 2014. Re-evaluation and extension of the MIS 5 tephrostratigraphy of the
888 Faroe Islands Region: the cryptotephras record. Palaeogeography, Palaeoclimatology,
889 Palaeoecology 409, 153-168.
890
891 Abbott, P.M., Bourne, A.J., Purcell, C.S., Davies, S.M., Scourse, J.D., Pearce, N.J.G., 2016.
892 Last glacial period cryptotephra deposits in an eastern North Atlantic marine sequence:
893 Exploring linkages to the Greenland ice-cores. Quaternary Geochronology 31, 62-76.
894
895 Abbott, P.M., Davies, S.M., Austin, W.E.N., Pearce, N.J.G., Hibbert, F.D., 2011.
896 Identification of cryptotephra horizons in a North East Atlantic marine record spanning
897 marine isotope stages 4 and 5a (~60,000-82,000 a b2k). Quaternary International 246, 177-
898 189.
899
900 Abbott, P.M., Griggs, A.J., Bourne, A.J., Chapman, M.R., Davies, S.M., in revision. Tracing
901 marine cryptotephras in the North Atlantic during the Last Glacial Period: Improving the
902 North Atlantic marine tephrostratigraphic framework. Submitted to Quaternary Science
903 Reviews.
904
905 Austin, W.E.N., Wilson, L.J., Hunt, J.B., 2004. The age and chronostratigraphical
906 significance of North Atlantic Ash Zone II. Journal of Quaternary Science 19, 137-146.
907
908 Berger, W., Heath, G.R., 1968. Vertical mixing in pelagic sediments. Journal of Marine
909 Research 26, 135-143.
910
911 Bigg, G.R., Wadley, M.R., Stevens, D.P., Johnson, J.A., 1996. Prediction of iceberg
912 trajectories for the North Atlantic and Arctic Oceans. Geophysical Research Letters 23, 3587-
913 3590.
914
915 Blockley, S.P.E., Edwards, K.J., Schofield, J.E., Pyne-O'Donnell, S.D.F., Jensen, B.J.L.,
916 Matthews, I.P., Cook, G.T., Wallace, K.L., Froese, D., 2015. First evidence of cryptotephra
917 in palaeoenvironmental records associated with Norse occupation sites in Greenland.
918 Quaternary Geochronology 27, 145-157.
919
920 Blockley, S.P.E., Pyne-O'Donnell, S.D.F., Lowe, J.J., Matthews, I.P., Stone, A., Pollard,
921 A.M., Turney, C.S.M., Molyneux, E.G., 2005. A new and less destructive laboratory
922 procedure for the physical separation of distal glass tephra shards from sediments. Quaternary
923 Science Reviews 24, 1952-1960.
924
925 Bourne, A.J., Cook, E., Abbott, P.M., Seierstad, I.K., Steffensen, J.P., Svensson, A., Fischer,
926 H., Schupbach, S., Davies, S.M., 2015. A tephra lattice for Greenland and a reconstruction of
927 volcanic events spanning 25-45 ka b2k. Quaternary Science Reviews 118, 122-141.
928

Brendryen, J., Haflidason, H., Sejrup, H.P., 2010. Norwegian Sea tephrostratigraphy of marine isotope stages 4 and 5: Prospects and problems for tephrochronology in the North Atlantic region. Quaternary Science Reviews 29, 847-864.

Davies, S.M., 2015. Cryptotephras: the revolution in correlation and precision dating. Journal of Quaternary Science 30, 114-130.

Davies, S.M., Abbott, P.M., Meara, Rh. H., Pearce, N.J.G., Austin, W.E.N., Chapman, M. R., Svensson, A., Bigler, M., Rasmussen, T.L., Rasmussen, S.O., Farmer, E.J., 2014. A North Atlantic tephrostratigraphical framework for 130-60 ka b2k: new tephra discoveries, marine-based correlations, and future challenges. Quaternary Science Reviews 106, 101-121.

Davies, S.M., Abbott, P.M., Pearce, N.J.P., Wastegård, S., Blockley, S.P.E., 2012. Integrating the INTIMATE records using tephrochronology: rising to the challenge. Quaternary Science Reviews 36, 11-27.

Davies, S.M., Elmquist, M., Bergman, J., Wohlfarth, B., Hammarlund, D., 2007. Cryptotephra sedimentation processes within two lacustrine sequences from west central Sweden. Holocene 17, 319-330.

Davies, S.M., Larsen, G., Wastegård, S., Turney, C.S.M., Hall, V.A., Coyle, L., Thordarson, T., 2010. Widespread dispersal of Icelandic tephra: how does the Eyjafjöll eruption of 2010 compare to past Icelandic events? Journal of Quaternary Science 25, 605-611.

Dokken, T.M., Jansen, E., 1999. Rapid changes in the mechanism of ocean convection during the last glacial period. Nature 401, 458-461.

Dyke, A.S., Andrews, J.T., Clark, P.U., England, J.H., Miller, G.H., Shaw, J., Veillette, J.J., 2002. The Laurentide and Innuitian ice sheets during the Last Glacial Maximum. Quaternary Science Reviews 21, 9-31.

Elliot, M., Labeyrie, L., Bond, G., Cortijo, E., Turon, J.-L., Tisnerat, N., Duplessy, J.-D., 1998. Millennial-scale iceberg discharges in the Irminger Basin during the last glacial period: Relationship with the Heinrich events and environmental settings. Paleoceanography 13, 433-446.

Elliot, M., Labeyrie, L., Dokken, T., Manthé, S., 2001. Coherent patterns of ice-rafted debris deposits in the Nordic regions during the last glacial (10-60 ka). Earth and Planetary Science Letters 194, 151-163.

Ezat, M.M., Rasmussen, T.L., Groeneveld, J., 2014. Persistent intermediate water warming during cold stadials in the southeastern Nordic seas during the past 65 k.y.. Geology 42, 663-666.

Funder, S., Kjeldsen, K.K., Kjær, K., Ó Cofaigh, C., 2011. The Greenland Ice Sheet during the past 30,000 years: a review. In Ehlers, J., Gibbard, P., Hughes, P.D. (eds) Quaternary Glaciations – Extent and Chronology: A Closer Look, pp. 699-714.

977 Gehrels, M.J., Lowe, D.J., Hazell, Z.J., Newnham, R.M., 2006. A continuous 5300-yr
978 Holocene cryptotephrostratigraphic record from northern New Zealand and implications for
979 tephrochronology and volcanic hazard assessment. Holocene 16, 173-187.
980
981 Griggs, A.J., Davies, S.M., Abbott, P.M., Coleman, M., Palmer, A.P., Rasmussen, T.L.,
982 Johnston, R., 2015. Visualising tephra sedimentation processes in the marine environment:
983 the potential of X-ray microtomography. Geochemistry, Geophysics, Geosystems 16, doi:
984 10.1002/2015GC006073.
985
986 Griggs, A.J., Davies, S.M., Abbott, P.M., Rasmussen, T.L., Palmer, A.P., 2014. Optimising
987 the use of marine tephrochronology in the North Atlantic: A detailed investigation of the
988 Faroe Marine Ash Zones II, III and IV. Quaternary Science Reviews 106, 122-139.
989
990 Gudmundsdóttir, E.R., Larsen, G., Björck, S., Ingólfsson, Ó., Striberger, J., 2016. A new
991 high-resolution Holocene tephra stratigraphy in eastern Iceland: Improving the Icelandic and
992 North Atlantic tephrochronology. Quaternary Science Reviews 150, 234-249.
993
994 Gudmundsson, M.T., Sigmundsson, F., Björnsson, H., Högnadóttir, T., 2004. The 1996
995 eruption at Gjálp, Vatnajökull ice cap, Iceland: efficiency of heat transfer, ice deformation
996 and subglacial water pressure. Bulletin of Volcanology 66, 46-65.
997
998 Hall, I.R., Colmenero-Hidalgo, E., Zahn, R., Peck, V.L., Hemming, S.R., 2011. Centennial-
999 to millennial-scale ice-ocean interactions in the subpolar northeast Atlantic 18-41 kyr ago.
1000 Paleoceanography 26, PA2224.
1001
1002 Hayward, C., 2012. High spatial resolution electron probe microanalysis of tephras and melt
1003 inclusions without beam-induced chemical modification. The Holocene 22, 119-125.
1004
1005 Hibbert, F.D., Austin, W.E.N., Leng, M.J., Gatliff, R.W., 2010. British Ice Sheet dynamics
1006 inferred from North Atlantic ice-rafted debris records spanning the last 175 000 years.
1007 Journal of Quaternary Science 25, 461-482.
1008
1009 Hodder, A.P.W., Wilson, A.T., 1976. Identification and correlation of thinly bedded tephra:
1010 The Tirau and Mairoa Ashes. New Zealand Journal of Geology and Geophysics 19, 663-682.
1011
1012 Hoff, U., Rasmussen, T.L., Stein, R., Ezat, M.M., Fahl, K., 2016. Sea ice and millennial-scale
1013 climate variability in the Nordic seas 90 kyr ago to present. Nature Communications 7:12247.
1014
1015 Hopkins, J.L., Millet, M.A., Timm, C., Wilson, C.J.N., Leonard, G.S., Palin, J.M., Neil, H.,
1016 2015. Tools and techniques for developing tephra stratigraphies in lake cores: A case study
1017 from the basaltic Auckland Volcanic Field, New Zealand. Quaternary Science Reviews 123,
1018 58-75.
1019
1020 Höskuldsson, Á., Óskarsson, N., Pedersen, R., Grönvold, K., Vogfjörð, K., Ólafsdóttir, R.,
1021 2007. The millennium eruption of Hekla in February 2000. Bulletin of Volcanology 70, 169-
1022 182.
1023
1024 Höskuldsson, Á., Sparks, R.S.J., Carroll, M.R., 2006. Constraints on the dynamics of
1025 subglacial basalt eruptions from geological and geochemical observations at Kverkfjöll, NE-
1026 Iceland. Bulletin of Volcanology 68, 689-701.

Hughes, A.L.C., Gyllencreutz, R., Lohne, Ø.S., Mangerud, J., Svendsen, J.I., 2016. The last Eurasian ice sheets – a chronological database and time-slice reconstruction, DATED-1. Boreas 45, 1-45.

Jakobsson, S.P., 1979. Petrology of recent basalts of the Eastern Volcanic Zone, Iceland. Acta Naturalia Islandia 26, 1-103.

Jakobsson, S.P., Jónasson, K., Sigurdsson, I.A., 2008. The three igneous rock suites of Iceland. Jökull 58, 117-138.

Jennings, A.E., Grönvold, K., Hilberman, R., Smith, M., Hald, M., 2002. High-resolution study of Icelandic tephras in the Kangerlussuaq Trough, southeast Greenland, during the last deglaciation. Journal of Quaternary Science 17, 747-757.

Jessen, S.P., Rasmussen, T.L., 2015. Sortable silt cycles in Svalbard slope sediments 74-0 ka. Journal of Quaternary Science 30, 743-753.

Kaminski, E., Tait, S., Ferrucci, F., Martet, M., Hirn, B., Husson, P., 2011. Estimation of ash injection in the atmosphere by basaltic volcanic plumes: The case of the Eyjafjallajökull 2010 eruption. Journal of Geophysical Research 116, B00C02.

Kutzbach, J.E., Wright Jr., H.E., 1985. Simulation of the climate of 18,000 years BP: Results for the North American/North Atlantic/European sector and comparison with the geologic record of North America. Quaternary Science Reviews 4, 147-187.

Lacasse, C., 2001. Influence of climate variability on the atmospheric transport of Icelandic tephra in the subpolar North Atlantic. Global and Planetary Change 29, 31-55.

Lane, C.S., Brauer, A., Martín-Puertas, C., Blockley, S.P.E., Smith, V.C., Tomlinson, E.L., 2015. The Late Quaternary tephrostratigraphy of annually laminated sediments from Meerfelder Maar, Germany. Quaternary Science Reviews 122, 192-206.

Larsen, G., Eiríksson, J., 2008. Holocene tephra archives and tephrochronology in Iceland – a brief overview. Jökull 58, 229-250.

Lawson, I.T., Swindles, G.T., Plunkett, G., Greenberg, D., 2012. The spatial distribution of Holocene cryptotephras in north-west Europe since 7 ka: implications for understanding ash fall events from Icelandic eruptions. Quaternary Science Reviews 41, 57-66.

Le Maitre, R.W., Bateman, P., Dudek, A., Keller, J., Lameyre, Le Bas, M.J., Sabine, P.A., Schmid, R., Sorensen, H., Streckeisen, A., Woolley, A.R., Zanettin, B., 1989. A Classification of Igneous Rocks and Glossary of Terms. Blackwell, Oxford.

Lowe, D.J., 2011. Tephrochronology and its application: A review. Quaternary Geochronology 6, 107-153.

MacDonald, G.A., Katsura, T. 1964. Chemical composition of Hawaiian lavas. Journal of Petrology 5, 83-133.

Mackay, H., Hughes, P.D.M., Jensen, B.J.L., Langdon, P., Pyne-O'Donnell, S.D.F., Plunkett, G., Froese, D.G., Coulter, S., Gardner, J.E., 2016. A mid to late Holocene cryptotephra framework from eastern North America. Quaternary Science Reviews 132, 101-113.

Mackie, E., Davies, S.M., Turney, C.S.M., Dobbyn, K., Lowe, J.J., 2002. The use of magnetic separation techniques to detect basaltic microtephra in glacial-interglacial transition (LGIT; 15-10 ka cal. BP) sediment sequences in Scotland. Scottish Journal of Geology 38, 21-30.

Martrat, B., Grimalt, J.O., Shackleton, N.J., de Abreu, L., Hutterli, M.A., Stocker, T.F., 2007. Four Climate Cycles of Recurring Deep and Surface Water Destabilizations on the Iberian Margin. Science 317, 502-507.

Matthews, I.P., Trincardi, F., Lowe, J.J., Bourne, A.J., Macleod, A., Abbott, P.M., Andersen, N., Asioli, A., Blockley, S.P.E., Lane, C.S., Oh, Y.A., Satow, C.S., Staff, R.A., Wulf, S., 2015. Developing a robust tephrochronological framework for Late Quaternary marine records in the Southern Adriatic Sea: new data from core station SA03-11. Quaternary Science Reviews 118, 84-104.

Mayewski, P.A., Meeker, L.D., Whitlow, S., Twickler, M.S., Morrison, M.C., Bloomfield, P., Bond, G.C., Alley, R.B., Gow, A.J., Grootes, P.M., Meese, D.A., Ram, M., Taylor, K.C., Wumkes, W., 1994. Changes in Atmospheric Circulation and Ocean Ice Cover over the North Atlantic During the last 41,000 Years. Science 263, 1747-1751.

Obrochta, S.P., Crowley, T.J., Channell, J.E.T., Hodell, D.A., Baker, P.A., Seki, A., Yokoyama, Y., 2014. Climate variability and ice-sheet dynamics during the last three glaciations. Earth and Planetary Science Letters 406, 198-212.

Oddson, B., Gudmundsson, M.T., Larsen, G., Karlsdóttir, S., 2012. Monitoring of the plume from the basaltic phreatomagmatic 2004 Grímsvötn eruption application of weather radar and comparison with plume models. Bulletin of Volcanology 74, 1395-1407.

Óladóttir, B.A., Sigmarsson, O., Larsen, G., Devidal, J.-L., 2011. Provenance of basaltic tephra from Vatnajökull volcanoes, Iceland, as determined by major- and trace-element analyses. The Holocene 21, 1037-1048.

Payne, R., Gehrels, M., 2010. The formation of tephra layers in peatlands: An experimental approach. Catena 81, 12-23.

Peck, V.L., Hall, I.R., Zahn, R., Elderfield, H., 2008. Millennial-scale surface and sub-surface paleothermometry from the northeast Atlantic, 55-8 ka BP. Paleoceanography 23, PA3221.

Peck, V.L., Hall, I.R., Zahn, R., Elderfield, H., Grousset, F., Hemming, S.R., Scourse, J.D., 2006. High resolution evidence for linkages between NW European ice sheet instability and Atlantic Meridional Overturning Circulation. Earth and Planetary Science Letters 243, 476-488.

Petersen, G.N., Bjornsson, H., Arason, P., von Löwis, S., 2012. Two weather radar time series of the altitude of the volcanic plume during the May 2011 eruption of Grímsvötn, Iceland. Earth System Science Data 4, 121-127.

Pilcher, J.R., Hall, V.A., 1992. Towards a tephrochronology for the Holocene of the north of Ireland. The Holocene 2, 255-259.

Ponomareva, V., Polyak, L., Portnyagin, M., Abbott, P.M., Zelenin, E., Garbe-Schönberg, D., Vakhrameeva, P., (2018) "Holocene tephra from the Chukchi-Alaskan margin, Arctic Ocean: Implications for sediment chronostratigraphy and volcanic history", Quaternary Geochronology 45, 85-97.

Pouget, S., Bursik, M., Rogova, G., 2014. Tephra redeposition and mixing in a Lateglacial hillside basin determined by fusion of clustering analyses of glass-shard geochemistry. Journal of Quaternary Science 29, 789-802.

Pyle, D.M., 1989. The thickness, volume and grainsize of tephra fall deposits. Bulletin of Volcanology 51, 1-15.

Pyne-O'Donnell, S.D.F., Hughes, P.D.M., Froese, D.G., Jensen, B.J.L., Kuehn, S.C., Mallon, G., Amesbury, M.J., Charman, D.J., Daley, T.J., Loader, N.J., Mauquoy, D., Street-Perrott, F.A., Woodman-Ralph, J., 2012. High-precision ultra-distal Holocene tephrochronology in North America. Quaternary Science Reviews 52, 6-11.

Rasmussen, T.L., Thomsen, E., Moros, M., 2016. North Atlantic warming during Dansgaard-Oeschger events synchronous with Antarctic warming and out-of-phase with Greenland climate. Scientific Reports 6, 20535.

Rebesco, M., Hernandez-Molina, F., J., Van Rooij, D., Wåhlin, A., 2014. Contourites and associated sediments controlled by deep-water circulation processes: State-of-the-art and future considerations. Marine Geology 352, 111-154.

Rose, N.L., Golding, P.N.E., Batterbee, R.W., 1996. Selective concentration and enumeration of tephra shards from lake sediment cores. Holocene 6, 243-246.

Ruddiman, W.F., Glover, L.K., 1972. Vertical mixing of ice-rafted volcanic ash in North Atlantic sediments. Geological Society Bulletin 83, 2817-2836.

Sparks, R.S.J., Wilson, L., Sigurdsson, H., 1981. The pyroclastic deposits of the 1875 eruption of Askja, Iceland. Philosophical Transactions of the Royal Society of London, Series A 299, 241-273.

Steinhauser, G., Bichler, M., 2008. Adsorption of ions onto high silica volcanic glass. Applied Radiation and Isotopes 66, 1-8.

Stoner, J.S., Channell, J.E.T., Hillaire-Marcel, C., Kissel, C., 2000. Geomagnetic paleointensity and environmental record from Labrador Sea core MD95-2024: global marine sediment and ice core chronostratigraphy for the last 110 kyr. Earth and Planetary Science Letters 183, 161-177.

Todd, J.A., Austin, W.E.N., Abbott, P.M., 2014. Quantifying bioturbation of a simulated ash fall event. In Austin, W.E.N., Abbott, P.M., Davies, S.M., Pearce, N.J.G., Wastegård, S., (eds) Marine Tephrochronology, Geological Society of London Special Publication 398, 195-207.

Turney, C.S.M., 1998. Extraction of rhyolitic component of Vedde microtephra from minerogenic lake sediments. Journal of Palaeolimnology 19, 199-206.

Voelker, A.H.L., Haflidason, H., 2015. Refining the Icelandic tephrachronology of the last glacial period – The deep-sea core PS2644 record from the southern Greenland Sea. Global and Planetary Change 131, 35-62.

Watson, E.J., Swindles, G.T., Lawson, I.T., Savov, I.P., 2015. Spatial variability of tephra and carbon accumulation in a Holocene peatland. Quaternary Science Reviews 124, 248-264.

Weinelt, M., Vogelsang, E., Kucera, M., Pflaumann, U., Sarnthein, M., Voelker, A., Erlenkeuser, H., Malmgren, B.A., 2003. Variability of North Atlantic heat transfer during MIS 2. Paleoceanography 18, 1071.

Zawalna-Geer, A., Lindsay, J.M., Davies, S.M., Augustinus, P., Davies, S., Extracting a primary Holocene cryptotephra record from Pupuke maar sediments, Auckland, New Zealand. Journal of Quaternary Science 31, 442-457.

Table 1: Details of the North Atlantic marine core network investigated in this study. Approximate sedimentation rates cover the 60-25 cal ka BP period for the cores, except for MD04-2829CQ which covers the 41-25 cal ka BP period, and were calculated using existing age-depth models for the sequences or approximated based on ages for event markers e.g. Heinrich events and North Atlantic Ash Zone II.

Core	Location	Lat/Long	Water depth	Approx. average sedimentation rate (cm/ka)	Example references
JM04-25PC	Western Svalbard slope	77º 28´ N, 09º 30´ E	1880 m	10	Jessen et al. (2015)
M23485-1	Iceland Sea	76 º 54.9´ N, 17º 52.4´ W	1120 m	17	-
MD95-2010	Norwegian Sea	66º 41.05´ N, 04º 33.97´ E	1226 m	16	Dokken and Jansen (1999)
JM11-19PC	North Faroe Slope	62º 49´ N, 03º 52´ W	1179 m	11	Ezat et al. (2014); Griggs et al. (2014)
SU90-24	Irminger Basin	62º 40´ N, 37º 22´ W	2100 m	19	Elliot et al. (1998, 2001)
MD04-2829CQ	Rosemary Bank	58º 56.93´ N, 09º 34.30´ W	1743 m	20	Hall et al. (2011)
MD04-2822	Rockall Trough	56º 50.54´ N, 11º 22.96´ W	2344 m	14	Hibbert et al. (2010)
MD99-2251	Gardar Drift	57º 26´ N, 27º 54´ W	2620 m	11	-
MD95-2024	Labrador Sea	50º 12.40´ N, 45º 41.22´ W	3539 m	22	Stoner et al. (2000)
GIK23415-9	Northern North Atlantic	53º 10.7´ N, 19º 08.7´ W	2472 m	9	Weinelt et al. (2003)
MD01-2461	Porcupine Seabight	51º 45´ N, 12º 55´ W	1153 m	13	Peck et al. (2006, 2008)
MD04-2820CQ	Goban Spur	49º 05.29´ N, 13º 25.90´ W	3658 m	11	Abbott et al. (2016)
MD01-2444	Iberian Margin	37º 33.68´ N, 10º 08.53´ W	2637 m	23	Martrat et al. (2007)

Table 2: Summary of the shard profiles, characteristics, transportation and deposition processes of cryptotephra deposit types common to North Atlantic marine sequences between 60-25 cal ka BP. ★ = position of the isochron for deposit type.

Deposit type	Typical shard profile	Deposit type characteristics	Transport and deposition processes
TYPE 1 Low concentration peak	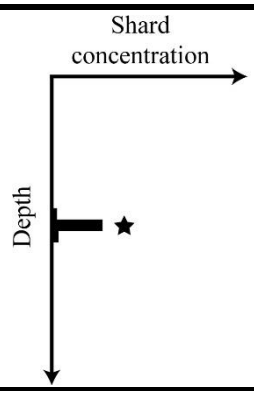	-Well constrained shard concentration peak -Low shard concentrations (< 50 per 0.5 g dws) -Shards generally 25-80 µm in diameter -Homogenous geochemical composition	-Single depositional event -Sourced from a single volcanic eruption -Potentially limited post-depositional reworking -Most likely primary airfall deposition
TYPE 2 High concentration peak	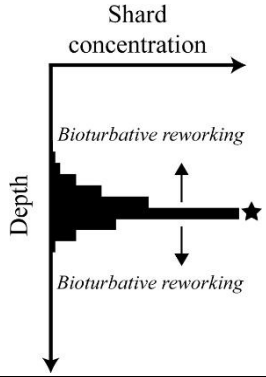	-Distinct peak in shard concentration -High shard concentrations (100s-1,000s per 0.5 g dws) -Upward and downward spanning up to 10 cm -Homogenous (Type 2A) or heterogeneous (Type 2B) geochemical composition	-Analysis of geochemistry, shard sizes and IRD required -Bioturbative reworking -Single depositional event -Transport via primary airfall, sea-ice and iceberg rafting possible
TYPE 3 High concentration peak; gradational upward tail	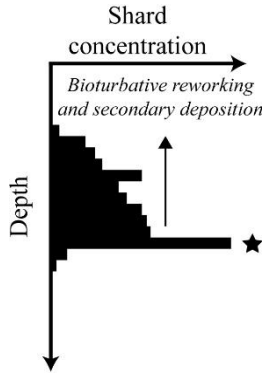	-Flat bottomed profile with a clear gradational upward tail -Very high shard concentrations (100,000s-1,000,000 per 0.5 g dws) -Deposit spread up to 100 cm -Homogenous composition of shards in peak	-Single depositional and volcanic event -Reworking via secondary deposition and bioturbation -Transport via primary airfall or sea-ice rafting -Useful isochron
TYPE 4 Diffuse distribution; multiple peaks	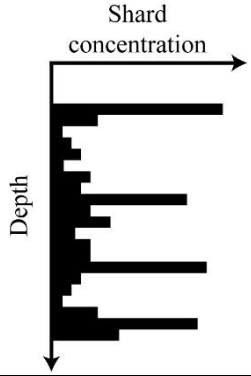	-High shard concentrations (1,000s-1,000,000s per 0.5 g dws) -Multiple peaks in concentration in a period of elevated shard concentrations -Deposit spread of 10s of cms -Heterogeneous geochemical composition common between peaks	-Deposition of multiple closely spaced eruptions or deposition via iceberg rafting -Comparison to Greenland tephra framework and IRD records required -Potential as regional marine-marine tie-lines
TYPE 5 Background of consistent concentration	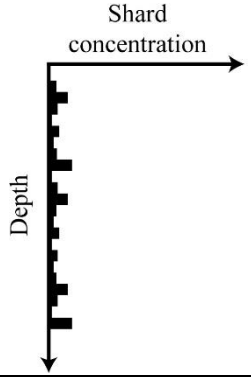	-Consistent deposition of shards with limited variability in concentrations between samples -Wide variability of deposit spreads -Heterogeneous or geochemically related to underlying deposits	-Background signal of glass shards -Shards reworked and remobilised in the oceanic system -Potential masking of low concentration glass shard deposits

Figure 1

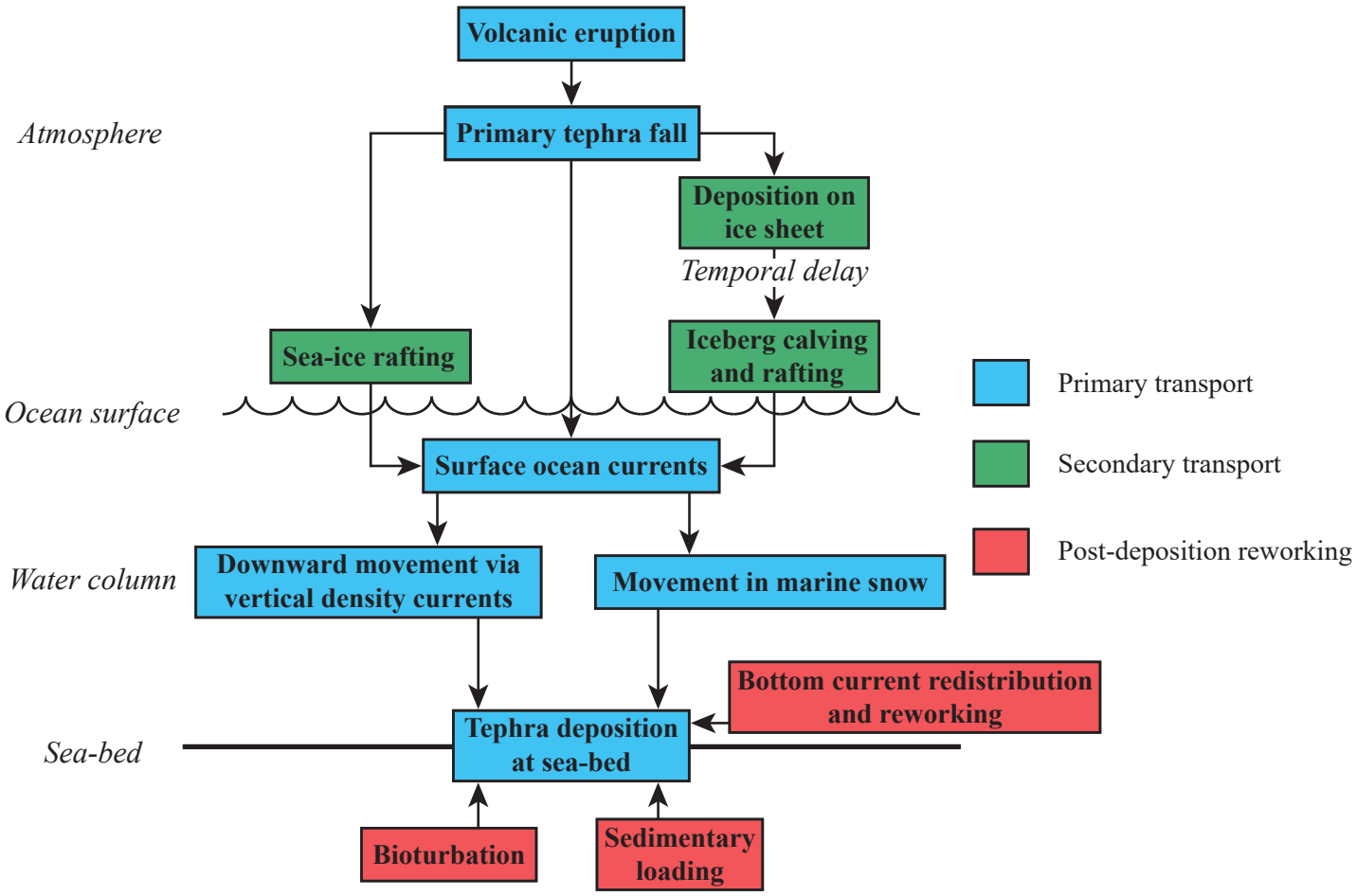
Volcanic eruption
Atmosphere
Primary tephra fall
Deposition on ice sheet
Temporal delay
Sea-ice rafting
Iceberg calving and rafting
Ocean surface
Surface ocean currents
Water column
Downward movement via vertical density currents
Movement in marine snow
Bottom current redistribution and reworking
Sea-bed
Tephra deposition at sea-bed
Bioturbation
Sedimentary loading
Primary transport
Secondary transport
Post-deposition reworking

Figure 2

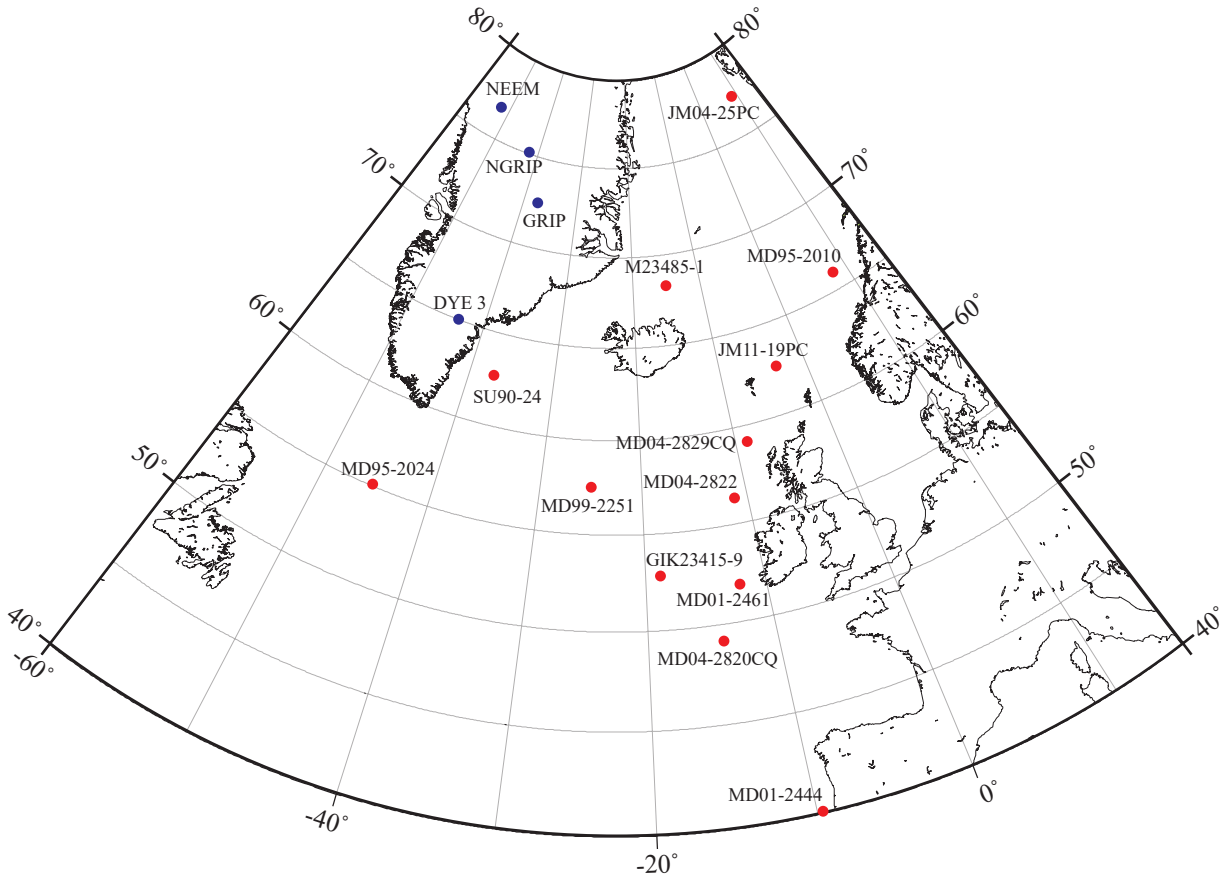
80°
80°
70°
70°
60°
60°
50°
50°
40°
-60°
-40°
-20°
0°
NEEM
NGRIP
GRIP
DYE 3
JM04-25PC
M23485-1
MD95-2010
JM11-19PC
SU90-24
MD04-2829CQ
MD95-2024
MD04-2822
MD99-2251
GIK23415-9
MD01-2461
MD04-2820CQ
MD01-2444

Figure 3

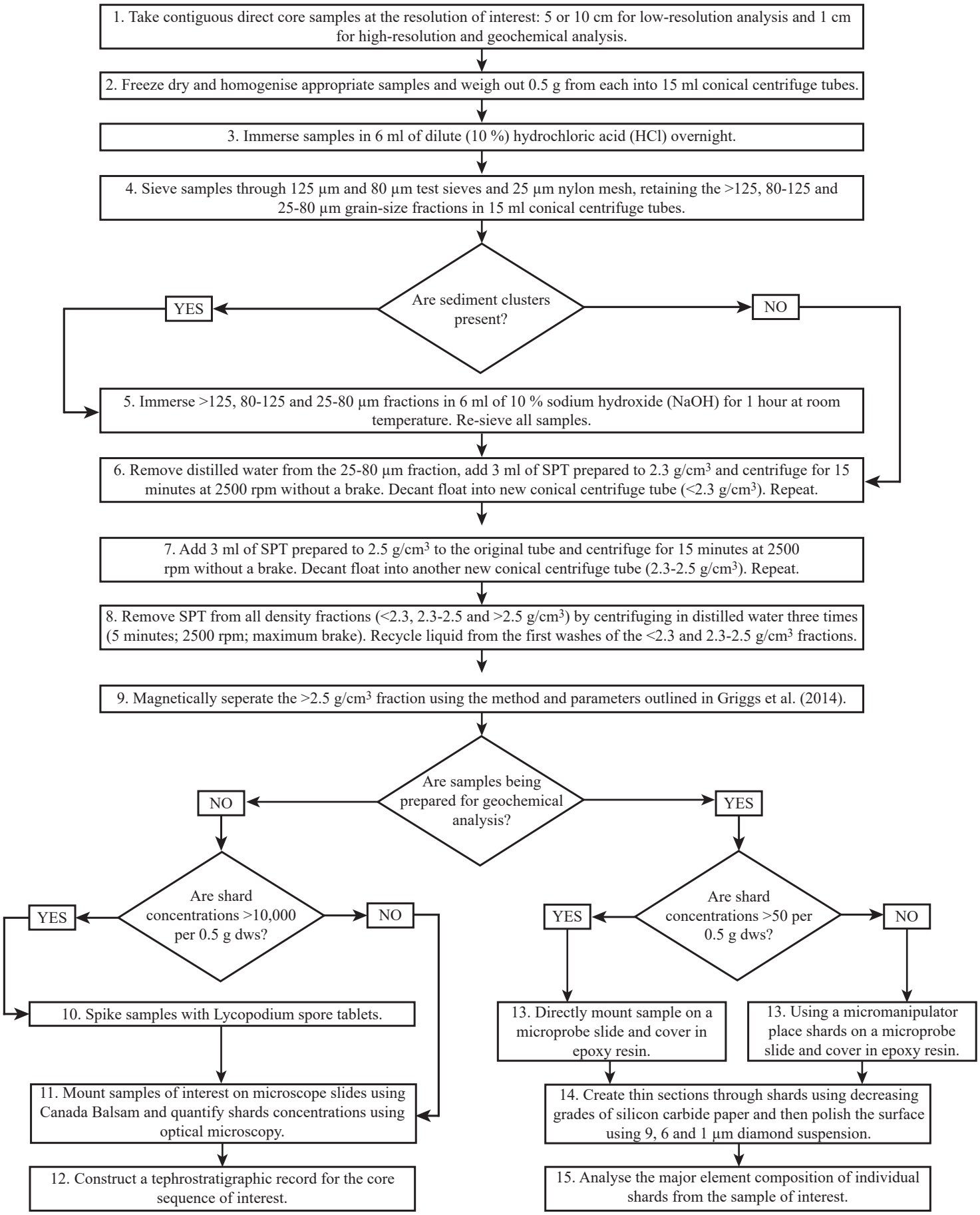
1. Take contiguous direct core samples at the resolution of interest: 5 or 10 cm for low-resolution analysis and 1 cm for high-resolution and geochemical analysis.
2. Freeze dry and homogenise appropriate samples and weigh out 0.5 g from each into 15 ml conical centrifuge tubes.
3. Immerse samples in 6 ml of dilute (10 %) hydrochloric acid (HCl) overnight.
4. Sieve samples through 125 µm and 80 µm test sieves and 25 µm nylon mesh, retaining the >125, 80-125 and 25-80 µm grain-size fractions in 15 ml conical centrifuge tubes.
Are sediment clusters present?
YES
NO
5. Immerse >125, 80-125 and 25-80 µm fractions in 6 ml of 10 % sodium hydroxide (NaOH) for 1 hour at room temperature. Re-sieve all samples.
6. Remove distilled water from the 25-80 µm fraction, add 3 ml of SPT prepared to 2.3 g/cm3 and centrifuge for 15 minutes at 2500 rpm without a brake. Decant float into new conical centrifuge tube (<2.3 g/cm3). Repeat.
7. Add 3 ml of SPT prepared to 2.5 g/cm3 to the original tube and centrifuge for 15 minutes at 2500 rpm without a brake. Decant float into another new conical centrifuge tube (2.3-2.5 g/cm3). Repeat.
8. Remove SPT from all density fractions (<2.3, 2.3-2.5 and >2.5 g/cm3) by centrifuging in distilled water three times (5 minutes; 2500 rpm; maximum brake). Recycle liquid from the first washes of the <2.3 and 2.3-2.5 g/cm3 fractions.
9. Magnetically seperate the >2.5 g/cm3 fraction using the method and parameters outlined in Griggs et al. (2014).
Are samples being prepared for geochemical analysis?
NO
YES
Are shard concentrations >10,000 per 0.5 g dws?
YES
NO
10. Spike samples with Lycopodium spore tablets.
11. Mount samples of interest on microscope slides using Canada Balsam and quantify shards concentrations using optical microscopy.
12. Construct a tephrostratigraphic record for the core sequence of interest.
Are shard concentrations >50 per 0.5 g dws?
YES
NO
13. Directly mount sample on a microprobe slide and cover in epoxy resin.
13. Using a micromanipulator place shards on a microprobe slide and cover in epoxy resin.
14. Create thin sections through shards using decreasing grades of silicon carbide paper and then polish the surface using 9, 6 and 1 µm diamond suspension.
15. Analyse the major element composition of individual shards from the sample of interest.

Figure 4

(a) Low resolution (5 cm) brown glass shard tephrostratigraphy for MD99-2251

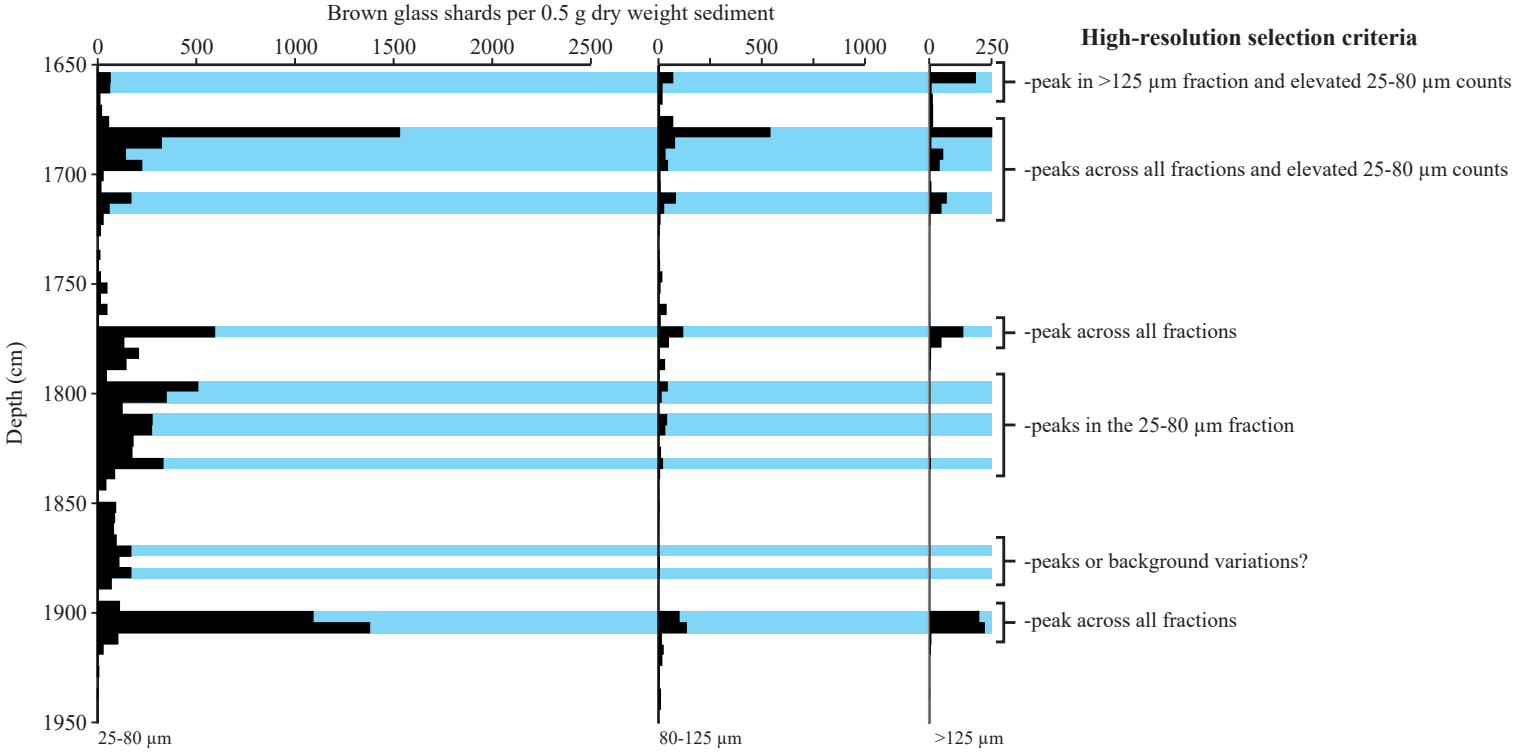

(b) Integrated high (1 cm) and low resolution (5 cm) brown glass shard tephrostratigraphy for MD99-2251

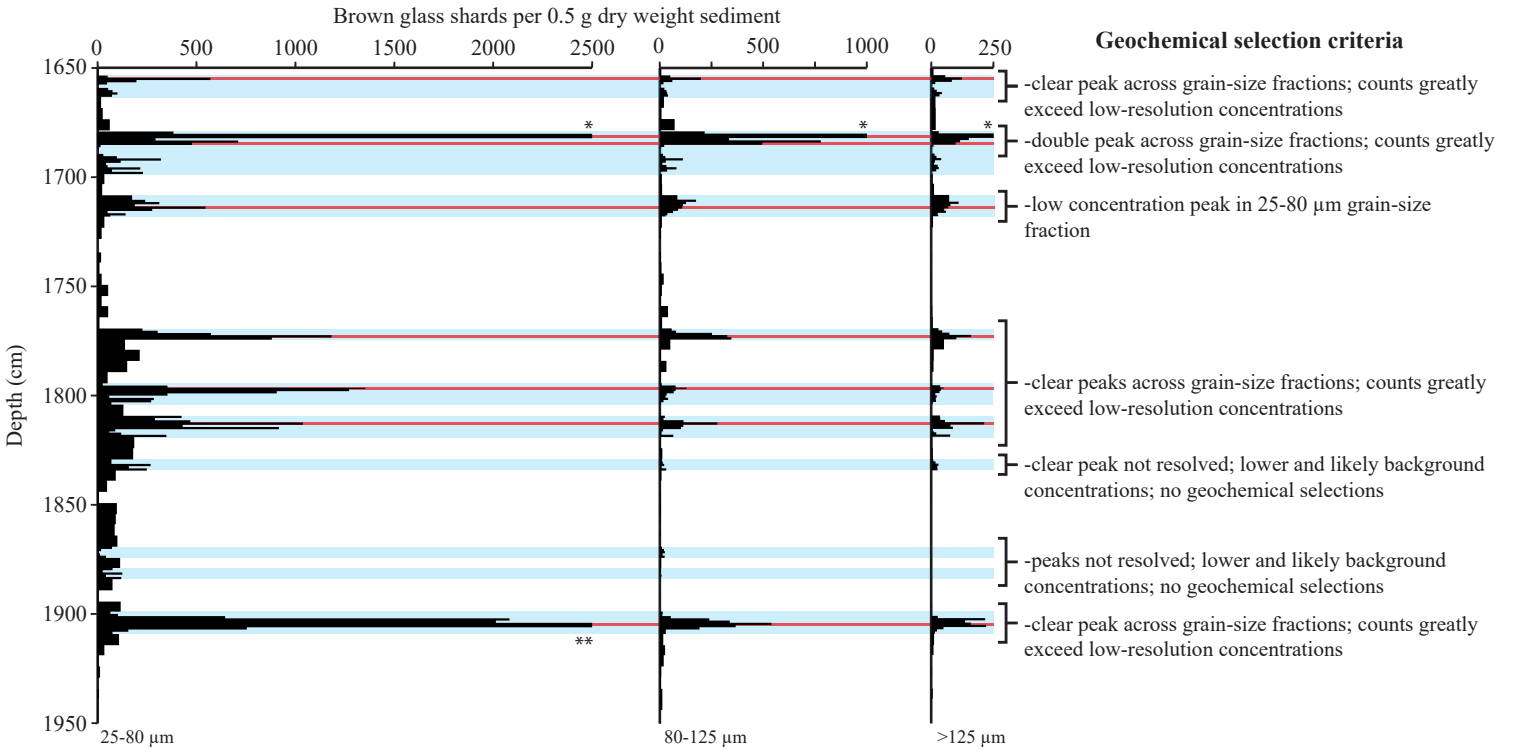

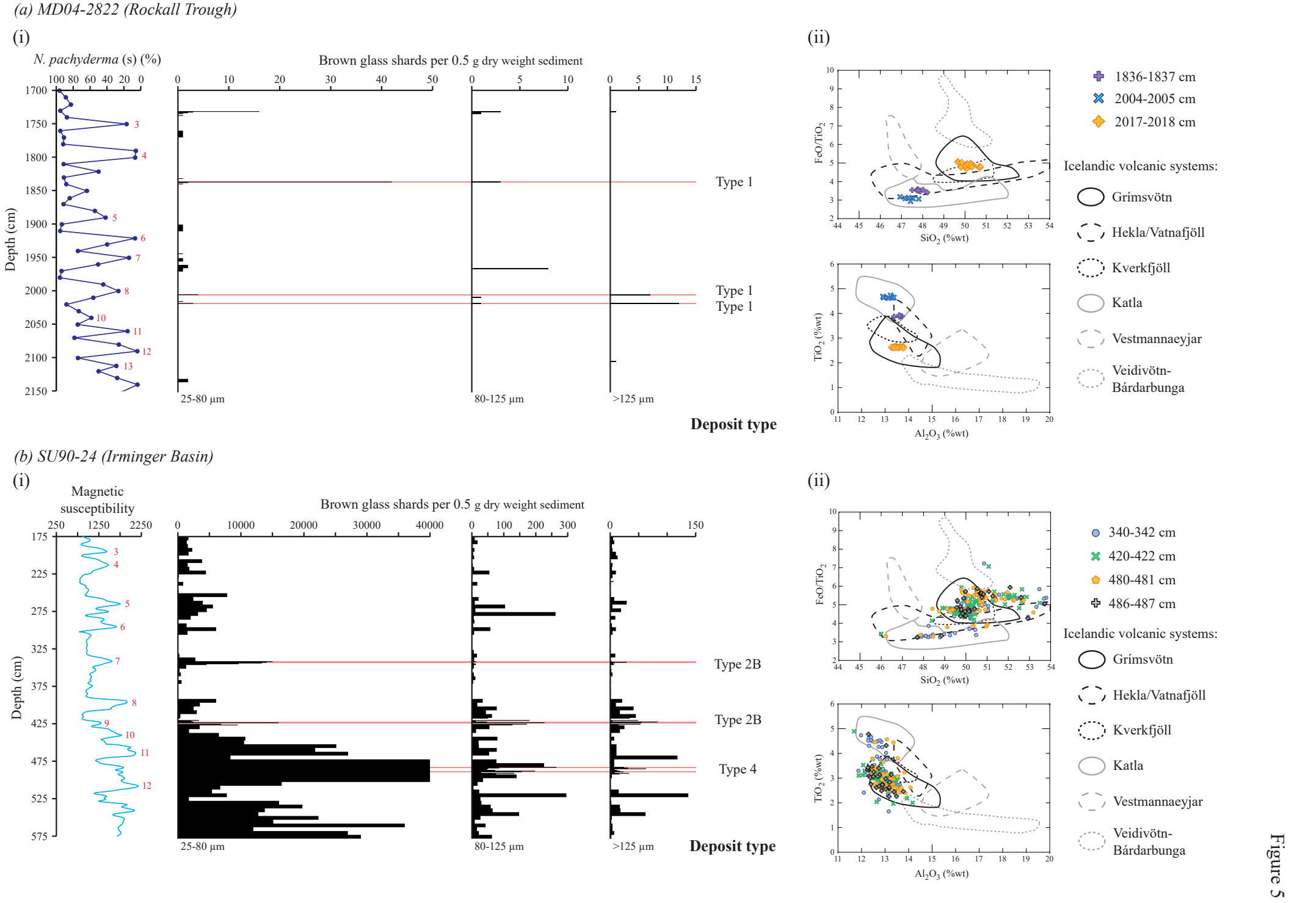
(a) MD04-2822 (Rockall Trough)
(i)
N. pachyderma (s) (%)
Brown glass shards per 0.5 g dry weight sediment
Depth (cm)
Type 1
Type 1
Type 1
25-80 µm
80-125 µm
>125 µm
Deposit type
(ii)
FeO/TiO2
SiO2 (%wt)
TiO2 (%wt)
Al2O3 (%wt)
1836-1837 cm
2004-2005 cm
2017-2018 cm
Icelandic volcanic systems:
Grímsvötn
Hekla/Vatnafjöll
Kverkfjöll
Katla
Vestmannaeyjar
Veidivötn-Bárdarbunga
(b) SU90-24 (Irminger Basin)
(i)
Magnetic susceptibility
Brown glass shards per 0.5 g dry weight sediment
Depth (cm)
Type 2B
Type 2B
Type 4
25-80 µm
80-125 µm
>125 µm
Deposit type
(ii)
FeO/TiO2
SiO2 (%wt)
TiO2 (%wt)
Al2O3 (%wt)
340-342 cm
420-422 cm
480-481 cm
486-487 cm
Icelandic volcanic systems:
Grímsvötn
Hekla/Vatnafjöll
Kverkfjöll
Katla
Vestmannaeyjar
Veidivötn-Bárdarbunga

Figure 5

(a)

(i) *MD95-2010 tephrostratigraphy - 910-920 cm - Type 2A deposit example*

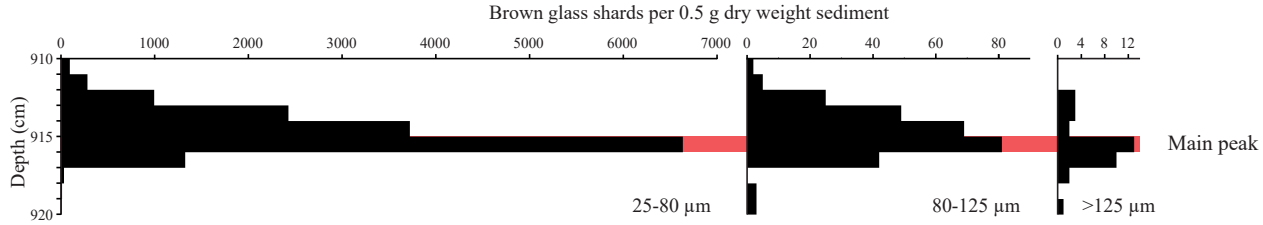

(ii) *MD95-2010 915-916 cm characterisation*

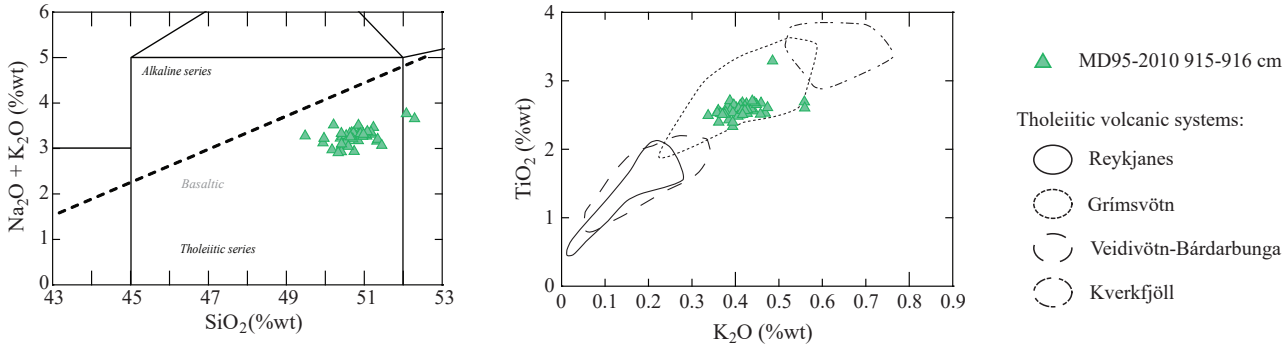

(b)

(i) MD01-2461 tephrostratigraphy - 940-950 cm - Type 2A deposit example

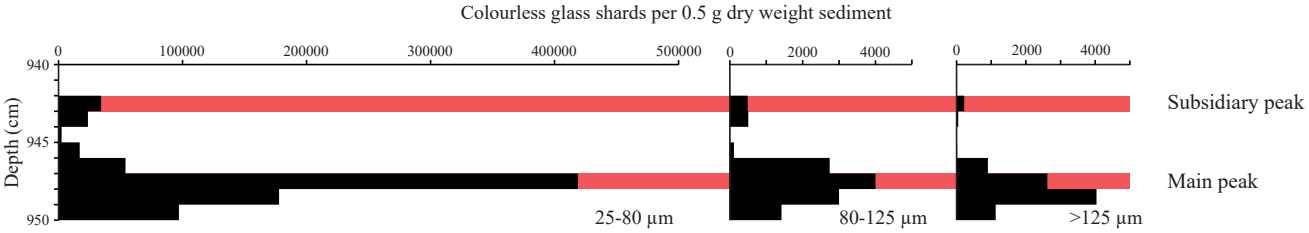

(ii) MD01-2461 947-948 cm characterisation

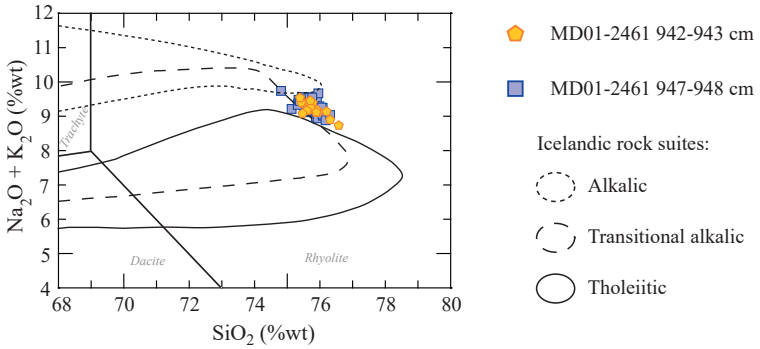

Figure 7

(a)

(i) *MD99-2251 tephrostratigraphy - 1950-2030 cm - Type 3 deposit example*

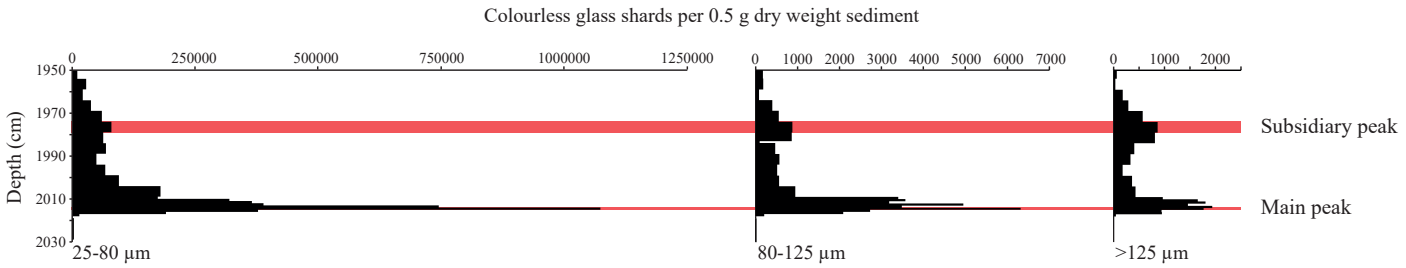

(ii) *MD99-2251 1974-1975 cm and 2014-2015 cm characterisation*

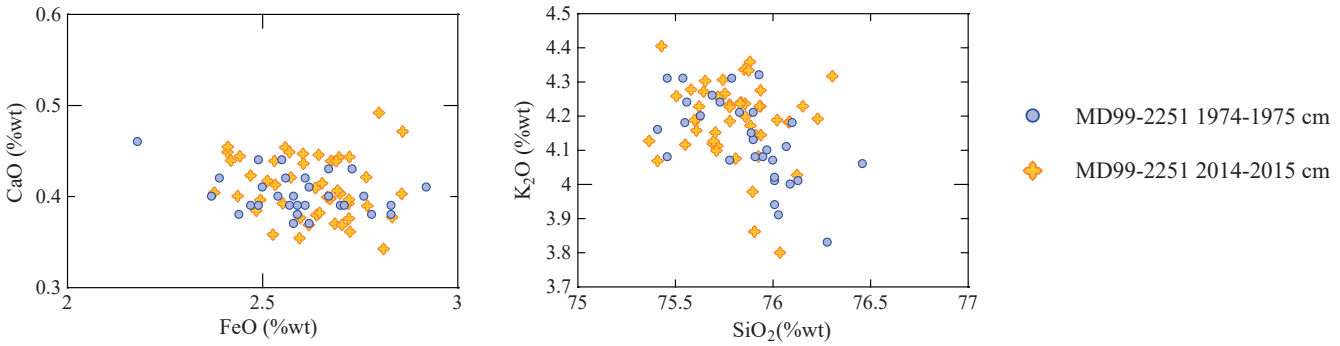

(b)

(i) *MD04-2820CQ tephrostratigraphy - 450-480 cm - Type 4 deposit example*

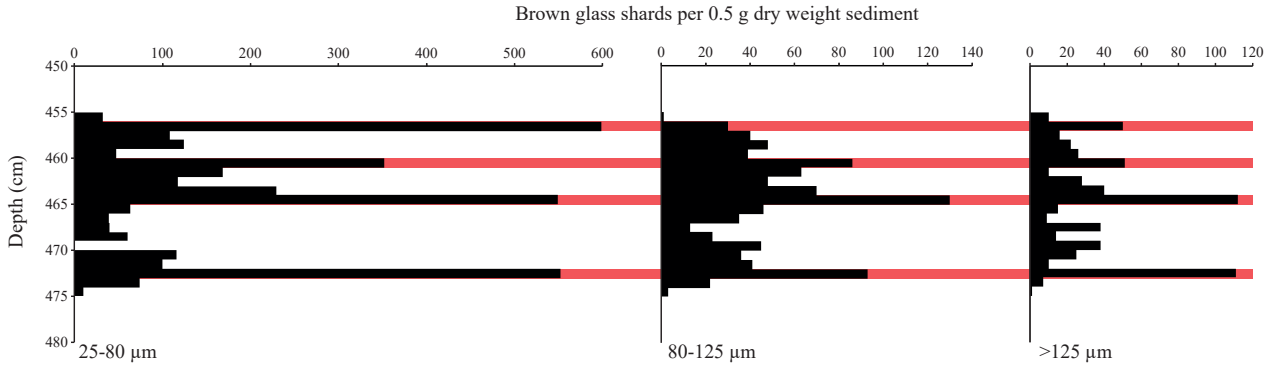

(ii) *MD99-2820CQ 456-473 cm characterisation*

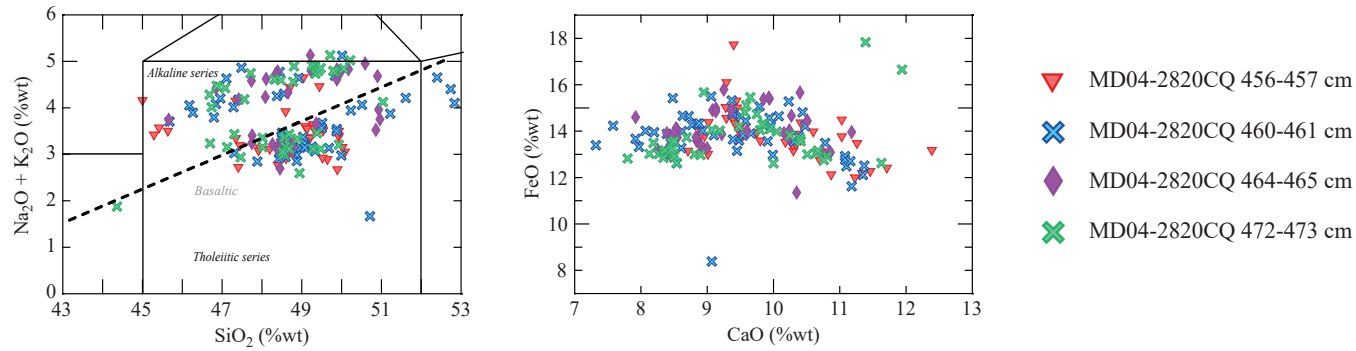

Figure 8

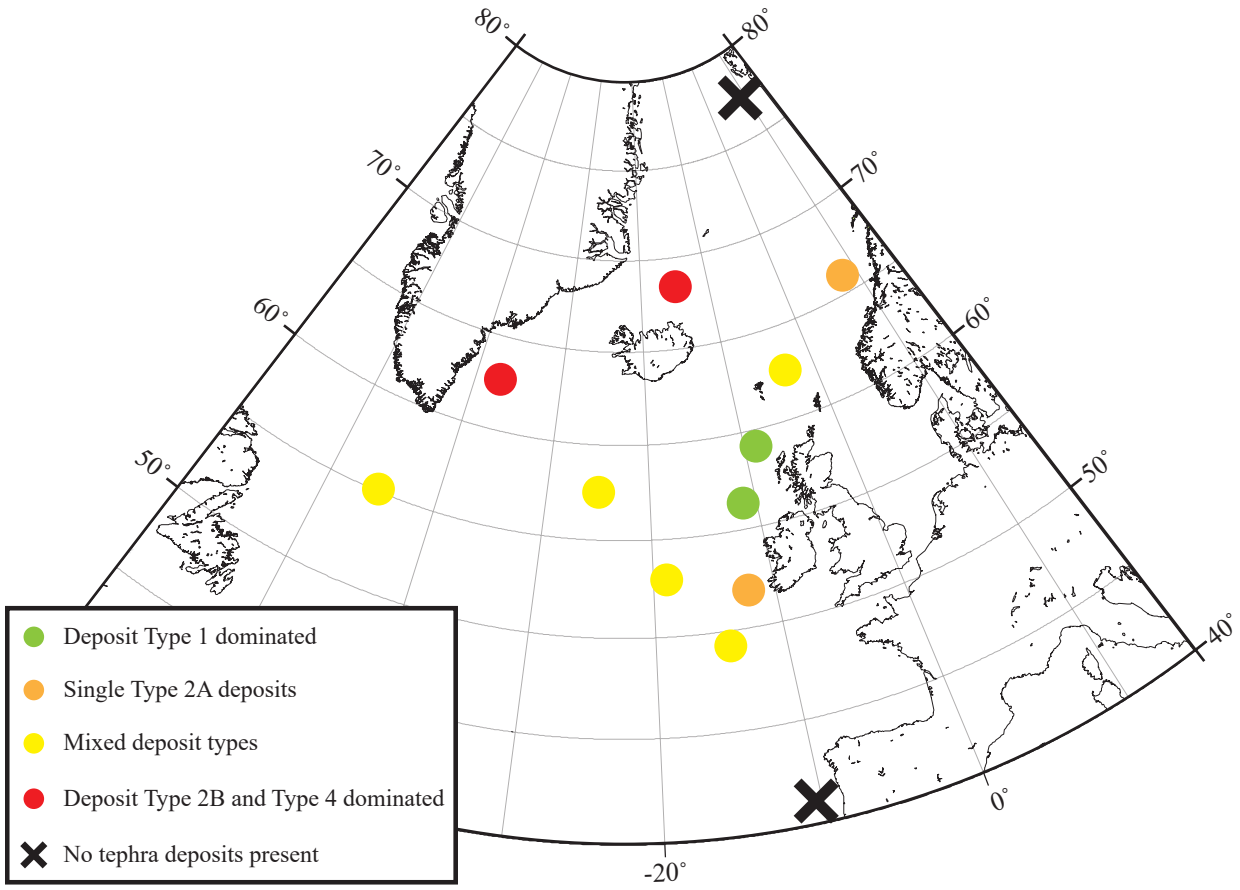
80°
80°
70°
70°
60°
60°
50°
50°
40°
0°
-20°
Deposit Type 1 dominated
Single Type 2A deposits
Mixed deposit types
Deposit Type 2B and Type 4 dominated
No tephra deposits present

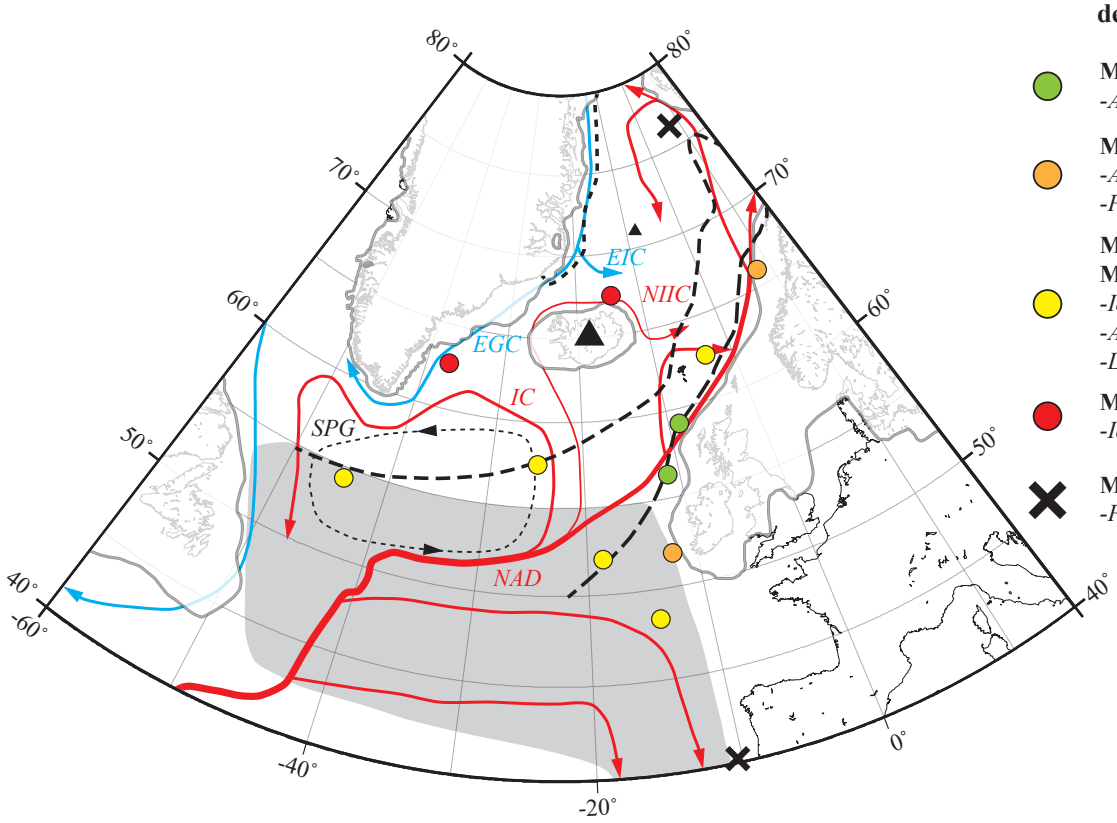

Primary controls on tephra deposition and preservation

MD04-2822, MD04-2829CQ
-Atmospheric dispersal patterns

MD95-2010, MD01-2461
-Atmospheric dispersal patterns
-Proximity to LGM ice-sheets

MD95-2024, MD99-2251, GIK23415-9, MD04-2820CQ, JM11-19PC
-Iceberg and sea-ice rafting
-Atmospheric dispersal patterns
-Lower sedimentation rates

M23485-1, SU90-24
-Iceberg rafting

MD01-2444, JM04-25PC
-Proximity to volcanic source

Ocean surface currents: *Warm* *Cold* *Subpolar Gyre*

Perennial sea-ice limit: *Interstadial* *Stadial* *Heinrich Event*

Volcanic centres | LGM ice-sheet limits | IRD Belt